A Scaling Law for Monocrystalline PV/T modules with CCPC and Comparison with Triple Junction PV Cells

W Li[1], M C Paul[1]*, M Rolley[2], T Sweet[2], M Gao[2], J Siviter[1], A Montecucco[1], A R Knox[1], H Baig[3], T K Mallick[3], E F Fernandez[4], G Han[5], D H Gregory[5], F Azough[6] and R Freer[6]

[1]School of Engineering, University of Glasgow, Glasgow, G12 8QQ, UK

[2]School of Engineering, Cardiff University, Cardiff, CF24 3AA, UK

[3]Environment and Sustainability Institute, University of Exeter, Penryn, TR10 9FE, UK

[4]Centre for Advanced Studies in Energy and Environment, University of Jaen, Jaen 23071, Spain

[5]WestCHEM, School of Chemistry, University of Glasgow, Glasgow, G12 8QQ, UK

[6]School of Materials, University of Manchester, Manchester, M13 9PL, UK

*Corresponding author's email: Manosh.Paul@glasgow.ac.uk

Tel: +44 (0) 141 330 8466

Abstract

Scaling laws serve as a tool to convert the five parameters in a lumped one-diode electrical model of a photovoltaic (PV) cell/module/panel under indoor standard test condition (STC) into the parameters under any outdoor conditions. By using the transformed parameters, a current-voltage curve can be established under any outdoor conditions to predict the PV cell/module/panel performance. A scaling law is developed for PV modules with and without crossed compound parabolic concentrator (CCPC) based on the experimental current-voltage curves of six flat monocrystalline PV modules collected from literature at variable irradiance and cell temperatures by using nonlinear least squares method. Experiments are performed to validate the model and method on a monocrystalline PV cell at various irradiances and cell temperatures. The proposed scaling law is compared with the existing one, and the former exhibits a much better accuracy when the cell temperature is higher than 40 ^{o}C. The scaling law of a triple junction flat PV cell is also compared with that of the monocrystalline cell and the CCPC effects on the scaling law are investigated with the monocrystalline PV cell. It is identified that the CCPCs impose a more significant influence on the scaling law for the monocrystalline PV cell in comparison with the triple junction PV cell. The proposed scaling law is applied to predict the electrical performance of PV/thermal modules with CCPC.

Keywords: scaling law, photovoltaic cell/module, roof-top system, one-diode electrical model, cell temperature, monocrystalline cell, crossed compound parabolic concentrator (CCPC)

1 Introduction

A photovoltaic (PV) module is subject to various climate conditions in its outdoor operation. PV manufactures usually provide a series of current-voltage (I-V) curves measured with standard indoor laboratory conditions at various solar irradiances, namely 1000, 800, 600, 400 and 200 W/m^2 and maintaining the cell temperature at 25 °C. Similarly, to evaluate the cell temperature effect on I-V curve, the curve is also measured at variable cell temperatures, namely 70, 50 and 25 °C under a fixed irradiance of 1000 W/m^2 in laboratory.

However, predicting the I-V curves of a PV module under outdoor conditions with variable solar irradiance and environmental effects poses significant challenges. Currently there are four different approaches to tackle with this issue. In the first approach, a linear interpolation /extrapolation method can be used, and then the I-V curve measured at a specific irradiance with cell temperature is interpolated according to the measured I-V curve at STC (e.g. at 25 °C cell temperature, 1000 W/m^2 irradiance and AM1.5 solar spectrum) [1, 2]. In the second approach, a five-point translation method can be adopted [3]. In that method, the temperature and irradiance are correlated to the current and voltage at five points, namely the short circuit, maximum power point, two intermediate and open circuit points. The five-points are then traced at any given irradiance and cell temperature, and as shown in [3, 4] and in [5], an I-V curve can be established with improved correlations for the parameters with irradiance.

The third approach is a lumped model method based on five (one-diode model) or seven (two-diode model) physical parameters defining an I-V curve. All or parts of the curves are extracted analytically or numerically from a known I-V curve at the short circuit, maximum and open circuit points at STC. These parameters or a few of them are linked to the cell temperature and irradiance, empirically or analytically, with some correlations. Finally, an I-V curve at a given irradiance and cell temperature under an off-STC can be established with updated parameters with the aid of these correlations. An extensive work on this topic has been done so far by using three points. For example, a simple method is presented in [6] to extract the five parameters from three points. Whereas, an iterative approach is proposed in [7] to extract the five parameters with the predicted maximum power point (MPP) marching experimental results. Variable irradiance and open-circuit voltage are involved in the five parameter model performed by [8] that involves a trial-and-error method, while an explicit model is proposed in [9] to obtain the five parameters of PV panels based on three points. In [10], however, the model is combined with a scaling law with a constant temperature-dependent open-circuit coefficient and the five parameters are determined numerically based on the three points for flat PV panels.

The five-parameter model is improved by introducing variable irradiance and open-circuit voltage into the model equation and the five parameters are determined iteratively and applied to

predict the PV panel electrical performance under outdoor conditions in [11]. In [12], photo-current is considered an electrical model parameter and solved with the other five parameters and adjustable variable to consider the changes in irradiance and cell temperature from three points. Like [11], variable irradiance and open-circuit voltage are introduced into the model, then the five parameters are decided from three points, and finally the model is used to estimate a flat PV panel electrical performance under different irradiances and cell temperatures [13]. The determination of five parameters based on three points is transformed into constrained nonlinear optimization problem and then optimized by means of a generalized reduced gradient (GRG) algorithm [14]. Evolutionary algorithm is also applied into the determination of five parameters from three points, as shown in [15]. Important contributions to this method have also been made by [16-18]. In these studies, additional formulas were proposed to determine diode quality factor, n, lumped series resistance, R_s and shunt resistance, R_{sh}, analytically. Further, two additional formulas were also proposed in [18] for the diode reversal saturation current, one for the short circuit point and the other for the maximum power point. However, it was not clarified whether both the formulae can result in the same reversal saturation current.

Alternatively, the five parameters can also be extracted by means of a whole I-V curve. This fourth method is a least square curve fitting technique by which a series of I-V points are fitted with a lumped physical electrical model of a PV module by minimising the squared error between predicted and measured currents at all the measured voltages to determine the five model parameters. To achieve a better curve fitting, various optimisation algorithms, namely Newton model in [19], Levenberg-Marquardt method in [20], genetic algorithms in [21, 22], pattern search in [23, 24], bird mating optimizer in [25] and an improved artificial fish swarm algorithm in [26], have been utilized to conduct the minimising procedure.

The method for utilising the five parameters to scale an I-V curve under outdoor conditions is not only simple but also shows a clear physical significance, so it is increasingly applied in solar energy engineering. This method is adopted in this article.

The correlations of a one-diode or two-diode model parameters to the solar irradiance and cell temperature in the third and fourth methods are defined as the scaling law for the PV module. Currently, the I-V of a module is characterized indoors under STC, as outlined above. In order to produce an I-V curve and track the MPP under other operational conditions than STC, a scaling law needs to be sought. However, the scaling laws determined mentioned above are for flat PV modules only. To date, to the best of the authors' knowledge there appears to be no scaling law that can potentially be applicable to PV modules with crossed compound parabolic concentrator (CCPC). Effects of CCPC on scaling laws are therefore remaining unexamined, and it is also not clear whether multi-junction PV cells/modules share the same scaling law with monocrystalline PV cells/modules.

As a concentrating technique, compound parabolic concentrators (CPC) have increasingly been developed and applied in solar electricity generation [27, 28] and solar air conditioner/electricity installation [30]. This includes some innovative configurations such as CPC presented in [31], crossed compound parabolic concentrator (CCPC) in [32], rotationally asymmetrical CCPC in [33], and asymmetrical holographic lenses in [34]. CCPC is a concentrating device with as high as 84% optical efficiency to improve PV modules/panels electrical power [30]. Therefore, it has been involved in the new roof-top PV/T (thermal) systems for this Solar SUNTRAP research project. By using a suitable scaling law, it is anticipated that one can predict the output behaviour of a concentrating PV/T system (CPV/T), evaluate the technological design as well as promote the market expansion of CCPC devices.

In this article, we aim to establish a scaling law for a monocrystalline CPV/T module based on a known I-V curve by means of a one-diode electrical model. We study the effects of CCPC on the scaling law as well as examine whether multi-junction PV cells share the same scaling law with monocrystalline ones. At first, a series of I-V experiments on monocrystalline PV cells with and without CCPC are carried out. Then the method for establishing the scaling law proposed and validated with experiments on the monocrystalline PV cells. Thirdly, the CCPC effects on the scaling law are identified to result in a new scaling law based on the law extracted from the I-V curves of existing PV panels. Fourthly, the scaling law obtained is compared with the existing one and the difference in the scaling laws between the monocrystalline and triple junction PV cells is clarified. Finally, the proposed scaling law is applied to predict the electrical performance of two roof-top CPV/T systems, installed at the University of Exeter, Penryn campus, UK and the University of Jaen, Jaen, Spain, respectively, under outdoor conditions at a cell temperature of around 20 °C and 40 °C.

2 Electrical Model and Scaling Law

2.1 Electrical model

Usually, an I-V curve for a typical single-junction PV module under STC using a single diode equivalent circuit is expressed mathematically by the following relation with five lumped parameters, Eq.(1), including the photocurrent, I_{ph}, diode reversal saturation current, I_d, diode quality factor, n, lumped series resistance, R_s and shunt resistance, R_{sh}.

$$I = I_{ph} - I_d \left\{ \exp\left[\frac{q(V + R_s I)}{nkT} \right] - 1 \right\} - \frac{V + R_s I}{R_{sh}} \tag{1}$$

Where V and I are the output voltage and current of the module respectively, q is the electron or elementary charge, $q = 1.6021766208\times10^{-19}$C, k is the Boltzmann constant, $k = 1.38064852\times10^{-23}$ J/K. I_{ph} depends on irradiance and a bit on cell temperature, while I_d is temperature-dependent only. Under STC, the five parameters are denoted by I_{sh0}, I_{d0}, n_0, R_{s0} and R_{sh0} at a cell temperature T_0, respectively, and Eq. (1) is rewritten as (2).

$$I = I_{sh0} - I_{d0}\left\{\exp\left[\frac{q(V+R_{s0}I)}{n_0 kT_0}\right]-1\right\} - \frac{V+R_{s0}I}{R_{sh0}} \tag{2}$$

There have been four methods for extracting the five lumped physical parameters of STC I-V curves as mentioned in the introduction. Here, as done in [35], the trust-region-reflective (TRR) least squares algorithm, which can handle bound constraints, is used to determine the five parameters of PV cell/module by minimising the following objective function in MATLAB.

$$f\left(I_{sh0}, I_{d0}, n_0, R_{s0}, R_{sh0}\right) = \sum_{i=1}^{N}\left[\left(I_i - I_i^{\exp}\right)V_i^{\exp}\right]^2 \tag{3}$$

where N is the number of experimental data points in I-V curve, I_i is the current calculated from Eq. (2) with a set of temporary five parameters at the i^{th} measured voltage $V_i^{\exp}$, and $I_i^{\exp}$ is the current at $V_i^{\exp}$.

Trust region denotes a subset of the region of an objective function which is approximated with a model function i.e. a quadratic function. The minimum objective function should be achieved in the trust region and in this method; the search step and size of trust region are decided and updated according to the ratio of the real change of the objective function to the predicted change in the objective function by the model function to ensure sufficient reduction of the objective function. Such procedures can result in the trust region out of one bound. Thus, the search direction should be reflected to the interior region constrained by the bounds with the law of reflection in optics on that bound. Compared to the Newton method and Levenberg-Marquardt algorithms, the trust region reflective method can ensure the optimization iteration remaining in the strict feasible region with a 2^{nd}-order convergence rate [36].

Once a set of five parameters are settled, the maximum electrical power will be tracked by minimizing the following objective function with TRR

$$f\left(I_{\max}, V_{\max}\right) = \frac{1}{IV} \tag{4}$$

where $I_{\max}$ and $V_{\max}$ are respectively the current and voltage at which a maximum electrical power, $P_{\max}$, is achieved.

Potential error associated with the I-V curve measurements will naturally have an impact in each of the fitted five parameters. Thus, an estimation of the standard error/deviation from its true value of these parameters is most important. In this work, the bootstrap method [37], i.e. resampling procedure, is utilised to resample the original experimental data for 500 times at every experimental point by using the *bootstrp* function in MATLAB. Then, 500 fitted five parameters are obtained by using these resampled data. Finally, the mean value and standard deviation of the five parameters are estimated by using the *mean* and *std* functions as well as *cov*, *corrcoef* for covariances and correlation coefficients in MATLAB.

2.2 Procedure for the new scaling law

The implementation of a scaling law depends on the method adopted to extract the five model parameters under STC. For example, if the method for the three points in an I-V curve is used, a set of relations specifying the change of short circuit, open circuit and maximum power points in response to a variable irradiance and cell temperature should be established beforehand. By using these relations, the new position of the three points can be decided for the variable irradiance and cell temperature. The new five parameters are extracted from the three positions to get the I-V curve at that irradiance and cell temperature.

Here we do not use this methodology. Instead, we extract the five electrical model parameters from a series of known scattered points of an experimental I-V curve at first, then we track the change of five parameters themselves with irradiance and cell temperature, in turn obtain the I-V curve under the known irradiance and cell temperature. Further, once the five parameters are decided based on a known irradiance and cell temperature, the I-V curve and its short circuit, maximum power and open circuit points are settled accordingly. In this circumstance, the following scaling law is proposed, Eq. (5), based on the existing proposals in [6, 9, 11, 12, 15].

$$\begin{cases} n = n_0 \\ R_s = \left(S_0/S\right)^{\nu} R_{s0} \\ R_{sh} = \left(S_0/S\right)^{\zeta} R_{sh0} \\ I_{ph} = \left(S/S_0\right)^{\xi}\left[I_{sh0} + \mu\left(T - T_0\right)\right] \\ I_d = I_{d0}\left(T/T_0\right)^{\gamma}\exp\left[\frac{1}{k}\left(E_0/T_0 - E/T\right)\right], \quad E = E_0\left[1 - 2.677\times10^{-4}\left(T - T_0\right)\right] \end{cases} \tag{5}$$

where four powers, ν, ζ , ξ and γ are determined by fitting the I-V curves at various irradiances and cell temperatures under an off STC, μ is the influence coefficient of cell temperature on I_{sh0} and can be found in a PV module datasheet or determined simply by a trial-and-error method, ζ represents the effect of irradiance on R_{sh}. It is shown that R_{sh} exhibited the least impact on an I-V curve [35] and our fitting excises also illustrated ζ value had an negligible effect on the fitted results. Hence, ζ =1 is held in the scaling law expressed by Eq. (5). Note that unit eV of E_0 and E should be converted into J with the relation: 1eV=1.6021766208×10^{-19} J when κ is in unit J/K in Eq. (5). The objective function for fitting the I-V curves at various irradiances and cell temperatures under off-STC is written as Eq.(6).

$$f\left(\nu,\xi,\gamma\right) = \sum_{j=1}^{M}\sum_{i=1}^{N_j}\left[\left(I_{ji} - I_{ji}^{\exp}\right)V_{ji}^{\exp}\right]^2 \tag{6}$$

Where j =1, 2, 3, 4 and 5 for 1000, 800, 600, 400 and 200 kW/m^2 irradiance respectively at 25 °C cell temperature, while j =6, 7, 8 for 25, 50 and 75 °C cell temperature respectively under 1 kW/m^2

irradiance. M is the total number of I-V curves measured, here M=8, N_j is the number of experimental points on an I-V curve under the j^{th} test condition, $I_{ji}^{\exp}$ and $V_{ji}^{\exp}$ are the current and voltage respectively at the i^{th} test point under the j^{th} test condition, and V_{ji} is the current given by Eq.(1) at $V_{ji}^{\exp}$. The TRR least squares algorithm is also used for the optimization of Eq.(6).

Once again, the bootstrap resampling procedure is applied to obtain the mean, standard deviation, co-variances and correlation coefficients of constants ν, ξ and γ.

3 Validation

At first, a series of experiments on the I-V curves of a monocrystalline 10×10 mm^2 sized bare PV cell and a cell with an optical CCPC of 3.6 geometrical concentration ratio (*CR*), i.e. the ratio of the CCPC inlet area over its outlet area, is carried out, see Fig. 1. The measurements were conducted under 1000, 800, 600 and 500 W/m^2 irradiances and at 25 and 50°C cell temperatures, respectively. The primary purpose of these experiments was to validate the model and methods used in the paper, and then identify the effects of CCPC on the scaling laws and also the differences in the laws between the PV modules and PV cells. The indoor experiments were conducted at Cardiff University.

In order to accurately electrically test the 10×10 mm^2 monocrystalline silicon (m-Si) CPV cell, a thermally optimised receiver was manufactured. This consisted of a copper plate with a centrally-located hole drilled for incorporating a thermocouple, a thermoelectric module (for accurate temperature control) directly bonded to the m-Si CPV cell. The CPV cell electrical contacts were carefully soldered on with attention being giving to eliminate shorting and cell damage wherever possible.

The multi-junction receivers consisted of a novel architecture; a sandwiched 2-PCB structure, allowing robust electrical and thermal testing. The smaller geometry III-V cell (active area 5.5 mm x 5.5mm) was thermally and electrically contacted to the thermoelectric module, with wirebonded top (n-type) contacts. The integrated PCB-CPV-TE device was mounted on a copper block for accurate temperature measurements (analogous to the m-Si receiver device architecture).

Experiments were done in a LOT Oriel LCS-100 94011A solar simulator to determine the performance of both the m-Si and triple-junction III-V CPV-TE receiver assemblies. A broadband solar spectrum of AM 1.5G, considered as the reference spectrum received from the sun, is used with wavelength range from 300 to 2500 nm [38], and hence can be considered representative for our testing. A Kipp and Zonen CM11 pyranometer was used to measure the global horizontal irradiance, with careful attention to keep it level due to the angular sensitivity of a pyranometer's operation. The dome was cleaned to eliminate dirt effects. The vertical height between the solar simulator lamp output and the pyranometer was carefully measured with attention given to obtaining a perpendicular reading. To correctly measure these devices, the 1000 W/m^2 standard irradiance plane was measured.

The top surface of the CPV cell was then placed at the centre of the defined irradiance plane to avoid any spatial uniformity errors of the irradiance, and to give highly reproducible results. The lamp height was adjusted after the CCPC optics were added to maintain the irradiance plane at the optical entrance to the device. The simulator was allowed a substantial warm-up time to avoid spectral or temporal anomalies.

The receiver assemblies were placed on a water heat exchanger for temperature stability and control, with the base of the receiver temperature measured using a k-type thermocouple. A very thin layer of thermal interface material was applied to maximise thermal conductivity from the device to the heat exchanger. Top solar cell surface temperature measurements were recorded with a FLIR-i7 thermal imaging camera with an emissivity set at 0.6. Without knowing the exact chemical composition of the AR coatings on the solar cells, or the thickness of the Sylguard encapsulant used, the surface emissivity cannot be quantified precisely. However, all of the pre-set emissivity settings on the FLIR thermal camera were tried (e.g. matt 0.95, semi-matt 0.8, semi-glossy 0.6 and glossy 0.3). The value 0.6 gave the closest agreement under the steady-state operation, with the k-type thermocouple integrated in the Cu block. For the "highest accuracy" the temperature measurements were taken immediately after the FLIR camera re-calibration. Contactless measurements, combined with thermocouple measurements, allowed evaluation of the thermal characteristics of the CPV-TE receiver without affecting irradiance levels on the cell.

The receivers were electrically connected using a four-wire measurement to an AUTOLAB system. I-V characteristics were measured inside of a blackened faraday cage to eliminate any light from the environment. The thermoelectric modules incorporated into both receiver assemblies were driven using an external power supply, with the current driven to a specific value to obtain the required cell temperature. This was chosen to be the control method due the proportionality between a thermoelectric's created temperature difference and the supplied current. Due to the thermoelectric module's temperature dependence (internal resistance, Seebeck co-efficient) Voltage temperature control was not used. The current input data to the receivers were highly reproducible.

To accurately calculate the confidence in the experimental readings, the equipment used in these data were evaluated and their manufacturer quoted uncertainties are collated. These are displayed in Table 1.

Secondly, the five parameters in Eq. (2) are decided by minimizing the objective function expressed by Eq. (3) in MATLAB by making use of TRR based on the I-V curve measured at STC. To evaluate the quality of the optimization based on the electrical power, the following root-mean-square-error (RMSE) is defined in Eq. (7).

$$\varepsilon_1 = \frac{\sqrt{\dfrac{\sum_{i=1}^{N_{STC}} \left[\left(I_{STCi} - I_{STCi}^{\exp} \right) V_{STCi}^{\exp} \right]^2}{N_{STC}}}}{\left(\dfrac{\sum_{i=1}^{N_{STC}} I_{STCi}^{\exp} V_{STCi}^{\exp}}{N_{STC}} \right)} \times 100\% \tag{7}$$

where N_{STC} is the number of scattered points in an experimental I-V curve at STC; $V_{STC}^{\exp}$ and $I_{STC}^{\exp}$ are the measured voltage and current at STC respectively, and I_{STC} is the predicted current at STC.

Thirdly, the scaling law expressed by Eq. (5) is applied to the measured I-V curves of the PV cell at off STC to decide the parameters such as ν, ζ, ξ and γ by minimizing the objective function, i.e. Eq. (6) with TRR. Similarly, a RMSE is defined as well to assess the quality of the optimization by using Eq. (8).

$$\varepsilon_2 = \frac{\sqrt{\dfrac{\sum_{j=1}^{M} \sum_{i=1}^{N_j} \left[\left(I_{ji} - I_{ji}^{\exp} \right) V_{ji}^{\exp} \right]^2}{\sum_{j}^{M} N_j}}}{\left(\dfrac{\sum_{j=1}^{M} \sum_{i=1}^{N_j} I_{ji}^{\exp} V_{ji}^{\exp}}{\sum_{j}^{M} N_j} \right)} \times 100\% \tag{8}$$

Note that the total number of experimental I-V curves used is $M = 6$. Note that the numerators of Eqs. (7) and (8) are the standard deviation of electric power, which is a measure to quantify the difference in the electrical power between prediction and measurement, and thus have nothing to do with the power magnitude itself. While the denominators of Eqs. (7) and (8) are the mean of the experimental electric power to make the standard deviation dimensionless. As a result, the curve fitting quality for various PV cells, modules and panels can be assessed with the same scale.

The five electrical parameters at STC and the four parameters for the scaling law have been summarized in Table 2 based on the experimental measurement data (with about 240 scattered points in an I-V curve). In the table the parameters are expressed with mean value ± standard deviation. The current- and power-voltage curves predicted by using the optimized five parameters at STC are compared with those of the measurements and illustrated in Fig.2. In the scaling law parametric optimization, the reference band gap of Si material, E_0 =1.121eV, at 25 °C, is held. Since the RMSE, ε_1, is as low as 0.61% as shown in Table 2, the agreement achieved between the measurement and the model prediction is considered to be excellent.

The current-voltage and power-voltage curves, estimated by the four parameters optimized for the scaling law as in Table 2, are also compared with the observations in Fig. 3 at variable

irradiance and cell temperature. The RMSE ε_2 is predicted to be as low as 2.05%, as presented in Table 2, thus confirming that the four optimized parameters result in a very good prediction of the current- and power-voltage curves under the off-STCs. Overall, the results above indicate the proposed models as well as the optimization algorithm used are sensible and provide results with a satisfactory prediction accuracy.

Generally, the standard deviations of five parameters in the electrical model or three constants in the scaling law is one-order smaller than the corresponding mean, and it is even lower for three constants in the scaling law.

A correlation coefficient of two variables is related to their covariance and defined by the following expression

$$\rho_{ab} = \frac{\mathrm{Cov}(a,b)}{\sigma_a \sigma_b} \tag{9}$$

where $\mathrm{Cov}(a,b)$ is the covariance of two variables, for the electrical model $a,b = R_{s0}, R_{sh0}, n_0, I_{d0}$ and I_{s0}, σ_a and σ_b are the standard deviations of two variables; for the scaling law, $a,b = \nu, \xi$ and γ. These statistic parameters can be estimated in MATLAB after least-squares optimizations are finished against the 500 data series resampled with the bootstrap method. The correlation coefficient matrices of the five parameters in the electrical model and three constants in the scaling law are listed below:

$$\begin{bmatrix}
1(\rho_{R_{s0}R_{s0}}) & -0.1041(\rho_{R_{s0}R_{sh0}}) & -0.2139(\rho_{R_{s0}n_0}) & -0.2085(\rho_{R_{s0}I_{d0}}) & 0.2261(\rho_{R_{s0}I_{sh0}}) \\
-0.1041(\rho_{R_{sh0}R_{s0}}) & 1(\rho_{R_{sh0}R_{sh0}}) & -0.1663(\rho_{R_{sh0}n_0}) & -0.1629(\rho_{R_{sh0}I_{d0}}) & -0.1049(\rho_{R_{sh0}I_{sh0}}) \\
-0.2139(\rho_{n_0R_{s0}}) & -0.1663(\rho_{n_0R_{sh0}}) & 1(\rho_{n_0n_0}) & 0.9947(\rho_{n_0I_{d0}}) & 0.0119(\rho_{n_0I_{sh0}}) \\
-0.2085(\rho_{I_{d0}R_{s0}}) & -0.1629(\rho_{I_{d0}R_{sh0}}) & 0.9947(\rho_{I_{d0}n_0}) & 1(\rho_{I_{d0}I_{d0}}) & 0.0541(\rho_{I_{d0}I_{sh0}}) \\
0.2261(\rho_{I_{sh0}R_{s0}}) & -0.1049(\rho_{I_{sh0}R_{sh0}}) & 0.0119(\rho_{I_{sh0}n_0}) & 0.0541(\rho_{I_{sh0}I_{d0}}) & 1(\rho_{I_{sh0}I_{sh0}})
\end{bmatrix} \tag{10}$$

And

$$\begin{bmatrix}
1(\rho_{\nu\nu}) & 0.0915(\rho_{\nu\xi}) & 0.0274(\rho_{\nu\gamma}) \\
0.0915(\rho_{\xi\nu}) & 1(\rho_{\xi\xi}) & 0.0379(\rho_{\xi\gamma}) \\
0.0274(\rho_{\gamma\nu}) & 0.0379(\rho_{\gamma\xi}) & 1(\rho_{\gamma\gamma})
\end{bmatrix} \tag{11}$$

It is found that in the electrical model, two parameters, n_0 and I_{d0}, are very strongly correlated, while for the other parameter pairs such as n_0 and R_{s0}, I_{d0} and R_{s0}, I_{sh0} and R_{s0}, a

weak correlation exists. The parameter R_{sh0} has no correlation to the other parameters. Thus, the influence of n_0 and I_{d0} on the current is the largest, the effect of R_{sh0} is the least, and the impact of the rest is in between. This outcome is in agreement with the results from the parametric sensitivity analysis presented in [35].

In the scaling law model, the off-diagonal correlation coefficients are two-order less the coefficients on diagonal. Therefore the parameters, ν, ξ and γ have no correlation and are independent to each other.

4 Results and discussion

4.1 Scaling law for the flat PV modules

Experimental data of six monocrystalline PV modules, namely BM60 265BB [39], Hyundai S325TI [40], Sanyo HIT215 [41], Shell SM50 [42], SILVANTIS D330 [6], and TSM270 DC05A [43] collected from literature and company datasheets, are involved to establish a new scaling law for the PV/T modules with CCPC (a new roof-top system described in Section 4.4). The I-V curves of theses PV modules are digitized by means of software and the number of scattered points in an I-V curve is around 12-30, which is in agreement with the data sheets of the National Institute of Standards and Technology (NIST) in Gaithersburg, Markland, USA [5].

At first, the five parameters of these PV modules are determined through an optimization process according to their I-V curves tested at STC, then the three powers are optimized against the experimental I-V curves under the off-STC conditions to get the scaling law. Note that the band gap, E_0=1.121eV for silicon at 25 °C, is imposed during the three-parameter optimization process. Finally, the average values of the three powers are deemed as the appreciate powers for the monocrystalline PV modules. In the first and second procedures, the bootstrap resampling method has been implemented to obtain statistic parameters of the variables in the electrical model and scaling law, respectively.

Table 3 presents the five parameters extracted with the corresponding RMSE ε_1 for the six PV modules under STC. The four model parameters for the scaling law are also illustrated in Table 3. Like Table 2, the optimized parameters are represented by their mean along with standard deviations. Because the experimental data with limited data points are taken from the PV module catalogue manual, which are not as smooth as our own experimental data, the RMSE ε_1 and ε_2 can be as large as 2.24% and 17.92%, respectively, in the worst cases.

A series of comparison are made in Figs. 4 to 6 between the model predictions and the measurements for the I-V curves and power-voltage curves at variable cell temperature and different irradiances. The largest difference from the experimental data is found at 600, 400 and 200 W/m^2

irradiances, which suggests that accurate experimental data of PV modules at low irradiances are needed. At three or four cell temperatures, the model predictions agree very well with the observations, indicating the model can cope with the cell temperature variation precisely.

The correlation coefficient matrices of the parameters in the electric model and the constants in the scaling law were extracted and expressed by (13) and (14), respectively, for the PV module BM60 265BB. These matrices for the rest PV panel are listed in Appendix.

$$\begin{bmatrix} 1(\rho_{R_{s0}R_{s0}}) & -0.2574(\rho_{R_{s0}R_{sh0}}) & 0.8582(\rho_{R_{s0}n_0}) & 0.8430(\rho_{R_{s0}I_{d0}}) & 0.5027(\rho_{R_{s0}I_{sh0}}) \\ -0.2574(\rho_{R_{sh0}R_{s0}}) & 1(\rho_{R_{sh0}R_{sh0}}) & -0.2925(\rho_{R_{sh0}n_0}) & -0.3033(\rho_{R_{sh0}I_{d0}}) & -0.2351(\rho_{R_{sh0}I_{sh0}}) \\ 0.8582(\rho_{n_0R_{s0}}) & -0.2925(\rho_{n_0R_{sh0}}) & 1(\rho_{n_0n_0}) & 0.9922(\rho_{n_0I_{d0}}) & 0.6034(\rho_{n_0I_{sh0}}) \\ 0.8430(\rho_{I_{d0}R_{s0}}) & -0.3033(\rho_{I_{d0}R_{sh0}}) & 0.9922(\rho_{I_{d0}n_0}) & 1(\rho_{I_{d0}I_{d0}}) & 0.6245(\rho_{I_{d0}I_{sh0}}) \\ 0.5027(\rho_{I_{sh0}R_{s0}}) & -0.2351(\rho_{I_{sh0}R_{sh0}}) & 0.6034(\rho_{I_{sh0}n_0}) & 0.6245(\rho_{I_{sh0}I_{d0}}) & 1(\rho_{I_{sh0}I_{sh0}}) \end{bmatrix} \tag{13}$$

And

$$\begin{bmatrix} 1(\rho_{\nu\nu}) & 0.0639(\rho_{\nu\xi}) & -0.1014(\rho_{\nu\gamma}) \\ 0.0639(\rho_{\xi\nu}) & 1(\rho_{\xi\xi}) & 0.0190(\rho_{\xi\gamma}) \\ -0.1014(\rho_{\gamma\nu}) & 0.0190(\rho_{\gamma\xi}) & 1(\rho_{\gamma\gamma}) \end{bmatrix} \tag{14}$$

For the parameters in the electric model, there is a significant correlation between n_0 and I_{d0}, R_{s0} and n_0, I_{d0} and R_{s0}, there is a certain correlation between I_{sh0} and n_0, I_{sh0} and I_{d0}, however, there is a weakened correlation. Once again R_{sh0} has no correlation to the other parameters. For the constants in the scaling law, there is no correlation between any of the two different constants. Compared to the elements in the correlation coefficient matrix of (10) for the PV cell, the element magnitude off-diagonal is smaller than the corresponding element magnitude in (13) for PV modules.

4.2 Comparison with the existing scaling law

Existing scaling laws can be found in [6, 12, 44], and the most popular ones are written as

$$\begin{cases} n = n_0 \\ R_s = R_{s0} \\ R_{sh} = (S_0/S)R_{sh0} \\ I_{ph} = (S/S_0)\left[I_{sh0} + \mu(T - T_0)\right], \ \mu = 3.74\times10^{-3} \\ I_d = I_{d0}(T/T_0)^3 \exp\left[\frac{1}{k}\left(\frac{E_0}{T_0} - \frac{E}{T}\right)\right], \ E = E_0\left[1 - 2.677\times10^{-4}(T - T_0)\right] \end{cases} \tag{15}$$

In comparison with the mean values of the four parameters of the six PV modules extracted are shown in Table 4, and it is seen that the scaling laws for the electric model variables n and R_{sh} are the same as those in Eq. (15). However, for the rest of the variables, they are different, especially

for variable I_d. For R_s and R_{sh}, the extracted mean power values are 0.6583 and 0.9087 compared with 1 in Eq. (15). For I_d, the extracted value is -13.3337 compared with 3 in Eq. (9).

To examine the effectiveness of the existing scaling laws of Eq. (15), we choose the Shell SM55 randomly as an example for this purpose. Fig. 7 illustrates the predicted I-V and Power-V curves against the experimental data. The predicted I-V and power-V curves at variable irradiances at 25 °C cell temperature seem reasonably good, but the predicted I-V curves at 40 °C and 60 °C cell temperatures and constant 1000 W/m^2 irradiance are very poor from the 'elbow' to the open circuit point, resulting in a 66.30% RMSE ε_2. This will lead to an under-estimated maximum electrical power and open circuit voltage.

4.3 Comparison of the scaling laws between a bare PV cell and a cell with CCPC

At first, the five parameters in the electric model expressed with Eq. (2), were extracted from the experimental I-V data of a bare flat PV cell without CCPC (i.e. *CR*=1), then the four parameters were decided using the scaling law in Eq. (5).These parameters have been shown in Table 2. For comparison between the different cases for the scaling laws, the four parameters are illustrated once again in Table 5 as Case 1.

Next, the six-parameters for the electric model of a PV cell with CCPC were decided by the experimental I-V curve. This model was proposed in [35] and is shown as follows

$$I = CR^m I_{sh0} - I_{d0}\left\{\exp\left[\frac{q(V+R_{s0}I)}{n_0 kT_0}\right]-1\right\} - \frac{V+R_{s0}I}{R_{sh0}} \tag{16}$$

where m is a newly introduced parameter named as an optical gain coefficient to be used to characterise the CCPC optical behaviour. Based on the extracted six parameters, the four parameters in the scaling laws were optimized against the measured I-V curve of the PV cell with CCPC (*CR*=3.6). These parameters are given in Table 5 as Case 1.

Thirdly, the six parameters in Eq. (16) were optimized based on the two I-V curves, one is for the bare PV cell without CCPC and the other is for the cell with CCPC, the details can be found in [35]. Finally, the four parameters in the scaling laws were determined letting *CR*=1 for the bare PV cell and *CR*=3.6 for the cell with CCPC. These parameters are tabulated in Table 5 as Case 2 and it is shown that the three parameters in the scaling laws such as ξ, ν and γ show a significant change from the bare PV cell to the cell with CCPC.

In average, ξ can be increased by 5%, ν by 15%, and γ by -20%, i.e. ξ=0.9542, ν =0.7570 and γ=-10.6670, while the other parameters ζ and μ remain unchanged. This fact suggests that the scaling laws based on bare PV modules are approximate to the PV modules with CCPC.

4.3 Comparison of the scaling laws between monocrystalline and triple junction PV cells

A series of experiments were also performed for the I-V curves of IQE PCB 2 triple junction bare PV cell. These cells are exploratory high efficiency cells based on GaInP/GaInAs/Ge materials which are being developed at IQE plc. The measurements were conducted under 1000, 800, 600 and 500 W/m^2 irradiance and at 25, 50 ^{o}C cell temperatures, respectively, for the bare PV cell and the cell with a CCPC on top. The five or six parameters in the electric model are extracted and the constants in the scaling laws are decided as well. In the scaling law's parameter optimization, the reference band gap of Ge material, E_0 =0.663eV at 25 ^{o}C, is held because Ge is the base material.

As shown in Table 6, the bare PV cell of IQE PCB 2 is subject to a quite different γ and μ in comparison with the bare cell of monocrystalline PV cell 100516 in Table 2, suggesting the triple junction PV cell is less affected by the cell temperature than a single junction silicon cell does. Further, it seems that the scaling law of the triple junction PV cell presented in Table 7 is less influenced by the CCPC compared with the monocrystalline PV cell 100516.

4.4 Application of the scaling law

The scaling law is applied to predict the electric performance of a newly developed CPV/T roof-top system as shown in Fig. 8. The system consists of four PV/T modules which include two flat PV/T modules (9×9flat and 2×2flat) and two PV/T modules with CCPC (9×9CCPC and 2×2CCPC), which are enclosed in a box with a top glass cover. The connections between these modules are illustrated in Fig. 8(b). PV cells used are made of monocrystalline Silicon with the cell sizes of 10mm×10mm for 9×9flat module and 9×9CCPC modules, 50.5mm×50.5mm for flat2x2 and 2×2CCPC modules. CCPCs are subject to the 3.6 concentration ratio with 84% optical efficiency. The fin heat exchangers installed under each of the PV modules are the same in structure, geometrical shape and dimensions as well as material. The extracted six parameters in the electric model of the four modules have been presented in [35] in indoor experiments.

An in-house quasi-steady multiphysics code is developed to predict both the electrical and thermal performances of the PV/T modules connected in a series by making using of the coupled lumped optical, electric and thermal models in MATLAB. In order to validate the scaling law proposed, an outdoor experimental study was conducted in Penryn campus, University of Exeter, England, on 17 September 2015. The measured solar irradiance incident onto the PV/T modules surface, ambient temperature and water temperature at the inlet of 9×9flat heat exchanger are presented in Fig. 9(a) in terms of the clock daytime at a given water flow rate of 4.3L/min. The monitored wind speed and ambient temperature are plotted as a function of time in Fig. 9(b). These data are used as an input into the code along with the optical, thermal property constants of the glass cover, silicon layer and absorber and flat module and incidence upon the four modules in terms of time as shown in Fig. 9(c). The incidence angle modifier (IAM) vs incidence relationship is presented

[45] and the optical efficiency of CCPC modules shown in Fig. 9(d) is predicted by ANSYS CFX., and then three cases are run.

In scenario 1, the scaling law for the flat PV modules without CCPC correction shown in Table 3 is involved. In scenario 2, the scaling laws for the flat PV modules but with CCPC correction, in which ξ is increased by 5%, ν by 30%, and γ by -20%; while the rest parameters ζ and ν remain unchanged, are embedded, i.e.

$$\begin{cases} n = n_0 \\ R_s = \left(S_0/S\right)^{\nu} R_{s0},\ \nu = 0.7570 \\ R_{sh} = \left(S_0/S\right)^{\zeta} R_{sh0},\ \zeta = 1 \\ I_{ph} = \left(S/S_0\right)^{\xi}\left[I_{sh0} + \mu\left(T - T_0\right)\right],\ \xi = 0.9542,\ \mu = 3.74\times10^{-3} \\ I_d = I_{d0}\left(T/T_0\right)^{\gamma}\exp\left[\frac{1}{k}\left(E_0/T_0 - E/T\right)\right],\ E = E_0\left[1 - 2.677\times10^{-4}\left(T - T_0\right)\right],\ \gamma = -10.6670 \end{cases} \tag{17}$$

In scenario 3, the existing scaling law expressed in Eq. (15) are activated. The cell temperature of the four modules is illustrated in Fig. 10(a). The temperature steadily rises from the first module 9×9flat to the last module 2×2CCPC, but it is not beyond 20 °C. The electric energy gained by the four modules is presented in Fig. 10(b). It is clear that the scaling law without CCPC correction can result in a significant error in the electric performance prediction for the PV/T module with CCPC. Once the law is corrected with the CCPC effect, the prediction approaches to the measurement. The prediction made by the existing scaling law, Eq. (15), is slightly poorer than the results produced by the proposed scaling law with CCPC effect correction.

The second example of application for the scaling law is the outdoor observation on the same roof-top system mentioned above made on 11 July 2016 at the Centro de Estudios Avanzados en Energía y Medio Ambiente (CEAEMA) in University of Jaen, southern Spain. The irradiance, ambient temperature, and the water temperature at the inlet of the heat exchanger of 9×9flat module as well as the incidence are shown in Fig. 11 in terms of time.

The predicted cell temperature in the four modules and the electric energy generated by the four modules are presented in Fig.12. The peak cell temperature can be as high as 42 ^{o}C. Once again, the prediction made by the scaling law with CCPC correction shows good agreement with the monitored result.

To the best of the authors' knowledge, the terminology scaling law for PV panel/module/cell appears to be named for the first time in solar energy engineering. In the paper, we collected the I-V data from existing PV modules under variable cell temperature and irradiance conditions firstly, then extracted the five parameters in the electric model, subsequently, the constants in the scaling law. Thus, the determined constants in the proposed scaling law are more practical and feasible. In addition, the CCPC effect on the law was considered with our experimental data. This idea is new and original.

As a result, the predicted electric energy obtained by the roof-top PV/T system was in better agreement with the measurement than the energy estimated by the existing scaling law.

Furthermore, by using this law the electric performance of a PV module/cell under outdoor conditions can be easily determined based on the performance under indoor condition. The proposed scaling law can also be applied to optimize the outdoor operation condition of PV/T modules.

It was shown the approach and algorithms used to extract the parameters in both the electric model and the scaling law are accurate and robust. They potentially can be adopted to establish the electric model and scaling law for other types of PV modules.

5 Conclusions

A set of scaling laws were proposed to convert the five parameters of electric model at STC to those obtained not under STC and subsequently to obtain the corresponding I-V curves. The constants in the scaling law are determined for the six monocrystalline PV modules by making use of the nonlinear least squares algorithm in MATLAB. The bootstrap resampling method was adopted to estimate statistic errors of the parameters in the electric model and the constants in the scaling law. The correlation coefficient matrices of these parameters and constants were discussed. The algorithm and method are validated by using the experimental I-V curves of a monocrystalline PV cell. These algorithms and methods are applied to the six PV modules and the corresponding five parameters are determined, and the new scaling law is put forward by taking the mean values of them. The law is compared with the existing scaling law. The effects of CCPC on the scaling law identified for monocrystalline Silicon and triple junction III-V PV cell are clarified. The existing scaling law leads to quite a large error in the I-V curves at high cell temperatures from the ‘elbow’ of the curve to the open circuit point. The scaling laws of monocrystalline PV cell are influenced more greatly by the CCPC than those of the triple junction PV cell. It is necessary to involve the CCPC effect into the scaling law.

6 Acknowledgments

The authors gratefully acknowledge the EPSRC Solar Challenge project SUNTRAP (EP/K022156/1) and Sêr Cymru National Research Network grant 152 for financial support. Grateful thanks are extended to IQE plc for supply of high efficiency III-V triple-junction CPV cells, and Cardiff University School of Physics for the use of cleanroom facilities.

References

[1] Tsuno Y, Hishikawa Y and Kurokawa K, Modelling of the I-V curves of the PV modules using linear interpolation/extrapolation, Solar Energy Materials & Solar cells, 2009, 93: 1070-1073.

[2] Polverini D, Tzamalis G and Mullejans H, A validated study of photovoltaic module series resistance determination under various operating conditions according to IEC 60891, Progress in Photovoltaics: Research and Applications, 2011, 20: 650-660.

[3] King D L, Boyson W E and Kratochvil J A, Photovoltaic array performance model, Sandia Report No. SAND2004-3535, Photovoltaic System R&D Department, Sandia National Laboratories, P. O. Box 5800, Albuquerque, New Mexico 87185-0752, USA.

[4] De Soto W, Klein S A and Beckman W A, Improvement and validation of a model for photovoltaic array performance, Solar Energy, 2006, 80: 78-88.

[5] Dongue S, Njomo D and Ebengai L, An improved nonlinear five-point model for photovoltaic modules, International Journal of Photoenergy, 2013, 11 pages.

[6] de Blas M A, Torres J L, Prieto E and Garcia A, Selecting a suitable model for characterizing photovoltaic devices, Renewable Energy, 2002, 25: 371-380.

[7] Villalva M G, Gazoli J R and Filho E R, Comprehensive approach to modelling and simulation of photovoltaic arrays, IEEE Transactions on Power Electronics, 2009, 24(5): 1198-1208.

[8] Lo Brano C, Orioli A, Ciulla G and Di Gangi A, An improved five-parameter model for photovoltaic modules, Applied Energy, 2010, 94: 1358-1370.

[9] Saloux E, Teyssedou A and Sorin M, Explicit model of photovoltaic modules to determine voltages and currents at the maximum power point, Solar Energy, 2011, 85: 713-722.

[10] Boyd M T, Klein S A, Reindl D T and Dougherty B P, Evaluation and validation of equivalent circuit photovoltaic solar cell performance models, ASME Journal of Solar Energy Engineering, 2011, 133: 021005-1-13.

[11] Lo Brano V, Orioli A and Ciulla G, On the experimental validation of an improved five-parameter model for silicon photovoltaic modules, Solar Energy Materials & Solar cells, 2012, 105:27-39.

[12] Dobos A P, An improved coefficient calculator for the California Energy Commission 6 parameter photovoltaic model, ASME Journal of Solar Energy Engineering, 2012, 134: 021011-1-6.

[13] Orioli A and Di Gangi A, A procedure to calculate the five-parameter model of crystalline silicon photovoltaic modules on the basis of the tabular performance data, Applied Energy, 2013, 102: 1160-1177.

[14] Lo Brano V and Ciulla G, An efficient analytical approach for obtaining a five parameters model of photovoltaic modules using only reference data, Applied Energy, 2013, 111: 894-903.

[15] Siddiqui M U nd Abido M, Parameter estimation for five-and seven-parameter photovoltaic electrical models using evolutionary algorithms, Applied Soft Computing, 2013, 13: 4608-4621.

[16] Carrero C, Rodriguez J, Ramirez D and Platero C, Simple estimation of PV modules loss resistances for low error modelling, Renewable Energy, 2010, 35: 1103-1108.

[17] Carrero C, Ramirez D, Rodriguez J and Platero C, Accurate and fast convergence method for parameter estimation of PV generators based on three main points of the I-V curve, Renewable Energy, 2011, 36: 2972-2977.

[18] Zhu X G, Fu Z H, Long X M and Li X, Sensitivity analysis and more accurate solution of photovoltaic solar cell parameters, Solar Energy, 2011, 85: 393-403.

[19] Easwarakhanthan T, Bottin J, Bouhouch I and Boutrit C, Nonlinear minimization algorithm for determining the solar cell parameters with microcomputers, International Journal of Solar Energy, 1986, 4: 1-12.

[20] Ikegami T, Maezono T, Nakanishi F, Yamagata and Ebihara K, Estimation of equivalent circuit parameters of PV module and its application to optimal operation of PV system, Solar Energy Materials & Solar Cells, 2001, 67: 389-395.

[21] Zagrouba M, Sellami A, Bouaicha M and Ksouri M, Identification of PV solar cells and modules parameters using the genetic algorithms: Application to maximum power extraction, 2010, 84: 860-866.

[22] Ismail M S, Moghavvemi M and Mahlia T M I, Characterization of PV module and global optimisation of its model parameters using genetic algorithm, Energy Conversion and Management, 2013, 73: 10-25.

[24] AlHajri M F, El-Naggar K M, AlRashidi M R and Al-Othman A K, Optimal extraction of solar cell parameters using pattern search, Renewable Energy, 2012, 44: 238-245.

[25] AlRashidi M R, AlHajri M F, El-Naggar K M, and Al-Othman A K, A new estimation approach for determining the I-V characteristics of solar cells, Solar Energy, 2011, 85:1543-1550.

[26] Askarzadeh A and Rezazadeh A, Extracting of maximum power point in solar cells using bird mating optimizer-based parameters identification approach, Solar Energy, 2013, 90:123-133.

[27] Han W, Wang H H and Chen L, Parameters identification for photovoltaic module based on an improved artificial fish swarm algorithm, The Scientific World Journal, Volume 2104, http://dx.doi.org/10.1155/2014/859239.

[28] Janjai S, Laksanaboonsong J and Seesaard T, Potential application of concentrating solar power systems for the generation of electricity in Thailand, Applied Energy, 2011, 83: 4960-4967.

[29] Desideri U, Zepparelli F, Morettini V and Garroni E, Comparative analysis of concentrating solar power and photovoltaic technologies: Technical and environmental evaluations, Applied Energy, 2013, 102: 765-784.

[30] Al-Alili A, Hwang Y, Radermacher R and Kubo I, A high efficiency solar air conditioner using concentrating photovoltaic/thermal collectors, Applied Energy, 2012, 93: 1380-147.

[31] Bahaidarah H M, Tanweer B, Gandhidasan P and et al, Experimental and numerical study on non-concentrating and symmetric unglazed compound parabolic photovoltaic concentration systems, Applied Energy, 2014, 136: 527-536.

[32] Sellami N and Mallick T K, Optical efficiency study of PV crossed compound parabolic concentrator, Applied Energy, 2013, 102: 868-876.

[33] Abu-Bakar S H, Muhammad-Sukki F and Ramirez-Iniguez R, et al, Rotationally asymmetrical compound parabolic concentrator for concentrating photovoltaic applications, Applied Energy, 2014, 136: 363-372.

[34] Chemisana D, Victoria Collados Mb, Quintanilla M and Atencia J, Holographic lenses for building integrated concentrating photovoltaics, Applied Energy, 2013, 110: 227-235.

[35] Li W, Paul M C and Sellami N, et al., Six-parameter electrical model for photovoltaic cell/module with crossed compound parabolic concentrator, Solar Energy, 2016, 137: 551-563.

[36] Li Y, Centering, trust region, reflective techniques for nonlinear minimization subject to bounds, Technical report-CTC93TR152, Cornell Theory Center, Cornell University, 1993.

[37] Chernick M R, Bootstrap Methods, New York: John Wiley and Sons , Inc, 1999, USA.

[38] http://lot-qd.com/products/light-lasers/solar-simulators/ [Accessed 31/03/16].

[39] https://es-media-prod.s3.amazonaws.com/media/u/35f/8f7/983 /93057e977697b62602c3bedfa1720649/B%20Series%20Datasheet.pdf

[40] http://aws-solar.com/wp-content/uploads/Datasheet-Hyundai-72-cell-TI-325W-mono.pdf

[41] http://eu-solar.panasonic.net/fileadmin/user_upload/downloads/technical_documents /Datasheet_214__215NKHE5_EN.pdf

[42] http://www.sunedison.com/sites/default/files/file-uploads/solar-material-resource/D-Series%2B72-Cell_dsv2_2014.pdf

[43] Xing W, Zhou J and Feng z, Effects of mounting geometries on photovoltaic module performance using CFD and single-diode model, Solar Energy, 2014, 103: pp.541–549.

[44] Siddiqui M U, Arif A F M, Kelly L and Dubowsky S, Three-dimensional thermal modelling of a photovoltaic module under varying condition, Solar Energy, 2012, 86: 2620-2631.

[45] Dynge A, Optical Modelling for Photovoltaic Panels, Master Thesis, University of Agder, Norway, 2013.

Appendix: Correlation Coefficient Matrices of Parameters in Electric Model and Constants in Scaling Law

For Hyundai S325TI PV module, the correlation coefficient matrix of five parameters in the electric model is as follows:

$$\begin{bmatrix} 1(\rho_{R_{s0}R_{s0}}) & 0.6230(\rho_{R_{s0}R_{sh0}}) & 0.9994(\rho_{R_{s0}n_0}) & 0.8351(\rho_{R_{s0}I_{d0}}) & 0.9782(\rho_{R_{s0}I_{sh0}}) \\ 0.6230(\rho_{R_{sh0}R_{s0}}) & 1(\rho_{R_{sh0}R_{sh0}}) & 0.6254(\rho_{R_{sh0}n_0}) & 0.4597(\rho_{R_{sh0}I_{d0}}) & 0.4967(\rho_{R_{sh0}I_{sh0}}) \\ 0.9994(\rho_{n_0R_{s0}}) & 0.6254(\rho_{n_0R_{sh0}}) & 1(\rho_{n_0n_0}) & 0.8472(\rho_{n_0I_{d0}}) & 0.9753(\rho_{n_0I_{sh0}}) \\ 0.8351(\rho_{I_{d0}R_{s0}}) & 0.4597(\rho_{I_{d0}R_{sh0}}) & 0.8472(\rho_{I_{d0}n_0}) & 1(\rho_{I_{d0}I_{d0}}) & 0.7892(\rho_{I_{d0}I_{sh0}}) \\ 0.9782(\rho_{I_{sh0}R_{s0}}) & 0.4967(\rho_{I_{sh0}R_{sh0}}) & 0.9753(\rho_{I_{sh0}n_0}) & 0.7892(\rho_{I_{sh0}I_{d0}}) & 1(\rho_{I_{sh0}I_{sh0}}) \end{bmatrix} \quad \text{(A1)}$$

And the matrix of the constants in the scaling law is as follows:

$$\begin{bmatrix} 1(\rho_{vv}) & 0.0072(\rho_{v\xi}) & -0.4546(\rho_{v\gamma}) \\ 0.0072(\rho_{\xi v}) & 1(\rho_{\xi\xi}) & 0.0325(\rho_{\xi\gamma}) \\ -0.4546(\rho_{\gamma v}) & 0.0325(\rho_{\gamma\xi}) & 1(\rho_{\gamma\gamma}) \end{bmatrix} \quad \text{(A2)}$$

Likewise, for the PV modules such as Sanyo HIT215, Shell SM55, SILVANTIS D330 and TSM270 DC05A, these correlation coefficient matrices are expressed by (A3) and (A4), (A5) and (A6), (A7) and (A8), (A9) and (A10), respectively:

$$\begin{bmatrix} 1(\rho_{R_{s0}R_{s0}}) & -0.3228(\rho_{R_{s0}R_{sh0}}) & -0.9015(\rho_{R_{s0}n_0}) & 0.8463(\rho_{R_{s0}I_{d0}}) & 0.3908(\rho_{R_{s0}I_{sh0}}) \\ -0.3228(\rho_{R_{sh0}R_{s0}}) & 1(\rho_{R_{sh0}R_{sh0}}) & -0.3644(\rho_{R_{sh0}n_0}) & -0.3728(\rho_{R_{sh0}I_{d0}}) & -0.2822(\rho_{R_{sh0}I_{sh0}}) \\ 0.9015(\rho_{n_0R_{s0}}) & -0.3644(\rho_{n_0R_{sh0}}) & 1(\rho_{n_0n_0}) & 0.9753(\rho_{n_0I_{d0}}) & 0.6217(\rho_{n_0I_{sh0}}) \\ 0.8463(\rho_{I_{d0}R_{s0}}) & -0.3728(\rho_{I_{d0}R_{sh0}}) & 0.9753(\rho_{I_{d0}n_0}) & 1(\rho_{I_{d0}I_{d0}}) & 0.6674(\rho_{I_{d0}I_{sh0}}) \\ 0.3908(\rho_{I_{sh0}R_{s0}}) & -0.2822(\rho_{I_{sh0}R_{sh0}}) & 0.6217(\rho_{I_{sh0}n_0}) & 0.6674(\rho_{I_{sh0}I_{d0}}) & 1(\rho_{I_{sh0}I_{sh0}}) \end{bmatrix} \quad \text{(A3)}$$

$$\begin{bmatrix} 1(\rho_{vv}) & 0.0062(\rho_{v\xi}) & 0.0811(\rho_{v\gamma}) \\ 0.0062(\rho_{\xi v}) & 1(\rho_{\xi\xi}) & 0.0225(\rho_{\xi\gamma}) \\ 0.0811(\rho_{\gamma v}) & 0.0225(\rho_{\gamma\xi}) & 1(\rho_{\gamma\gamma}) \end{bmatrix} \quad \text{(A4)}$$

And

$$\begin{bmatrix} 1(\rho_{R_{s0}R_{s0}}) & -0.2752(\rho_{R_{s0}R_{sh0}}) & 0.9207(\rho_{R_{s0}n_0}) & 0.8629(\rho_{R_{s0}I_{d0}}) & 0.4376(\rho_{R_{s0}I_{sh0}}) \\ -0.2752(\rho_{R_{sh0}R_{s0}}) & 1(\rho_{R_{sh0}R_{sh0}}) & -0.3324(\rho_{R_{sh0}n_0}) & -0.3393(\rho_{R_{sh0}I_{d0}}) & -0.2873(\rho_{R_{sh0}I_{sh0}}) \\ 0.9207(\rho_{n_0R_{s0}}) & -0.3324(\rho_{n_0R_{sh0}}) & 1(\rho_{n_0n_0}) & 0.9700(\rho_{n_0I_{d0}}) & 0.6404(\rho_{n_0I_{sh0}}) \\ 0.8629(\rho_{I_{d0}R_{s0}}) & -0.3393(\rho_{I_{d0}R_{sh0}}) & 0.9700(\rho_{I_{d0}n_0}) & 1(\rho_{I_{d0}I_{d0}}) & 0.6862(\rho_{I_{d0}I_{sh0}}) \\ 0.4376(\rho_{I_{sh0}R_{s0}}) & -0.2873(\rho_{I_{sh0}R_{sh0}}) & 0.6404(\rho_{I_{sh0}n_0}) & 0.6862(\rho_{I_{sh0}I_{d0}}) & 1(\rho_{I_{sh0}I_{sh0}}) \end{bmatrix} \tag{A5}$$

$$\begin{bmatrix} 1(\rho_{vv}) & 0.0235(\rho_{v\xi}) & 0.0585(\rho_{v\gamma}) \\ 0.0235(\rho_{\xi v}) & 1(\rho_{\xi\xi}) & 0.0045(\rho_{\xi\gamma}) \\ 0.0585(\rho_{\gamma v}) & 0.0045(\rho_{\gamma\xi}) & 1(\rho_{\gamma\gamma}) \end{bmatrix} \tag{A6}$$

And

$$\begin{bmatrix} 1(\rho_{R_{s0}R_{s0}}) & -0.2548(\rho_{R_{s0}R_{sh0}}) & 0.8593(\rho_{R_{s0}n_0}) & 0.8449(\rho_{R_{s0}I_{d0}}) & 0.3124(\rho_{R_{s0}I_{sh0}}) \\ -0.2548(\rho_{R_{sh0}R_{s0}}) & 1(\rho_{R_{sh0}R_{sh0}}) & -0.2613(\rho_{R_{sh0}n_0}) & -0.2688(\rho_{R_{sh0}I_{d0}}) & -0.2007(\rho_{R_{sh0}I_{sh0}}) \\ 0.8593(\rho_{n_0R_{s0}}) & -0.2613(\rho_{n_0R_{sh0}}) & 1(\rho_{n_0n_0}) & 0.9956(\rho_{n_0I_{d0}}) & 0.4964(\rho_{n_0I_{sh0}}) \\ 0.8449(\rho_{I_{d0}R_{s0}}) & -0.2688(\rho_{I_{d0}R_{sh0}}) & 0.9956(\rho_{I_{d0}n_0}) & 1(\rho_{I_{d0}I_{d0}}) & 0.5243(\rho_{I_{d0}I_{sh0}}) \\ 0.3124(\rho_{I_{sh0}R_{s0}}) & -0.2007(\rho_{I_{sh0}R_{sh0}}) & 0.4964(\rho_{I_{sh0}n_0}) & 0.5243(\rho_{I_{sh0}I_{d0}}) & 1(\rho_{I_{sh0}I_{sh0}}) \end{bmatrix} \tag{A7}$$

$$\begin{bmatrix} 1(\rho_{vv}) & -0.0249(\rho_{v\xi}) & -0.0067(\rho_{v\gamma}) \\ -0.0249(\rho_{\xi v}) & 1(\rho_{\xi\xi}) & 0.0417(\rho_{\xi\gamma}) \\ -0.0067(\rho_{\gamma v}) & 0.0417(\rho_{\gamma\xi}) & 1(\rho_{\gamma\gamma}) \end{bmatrix} \tag{A8}$$

And

$$\begin{bmatrix} 1(\rho_{R_{s0}R_{s0}}) & -0.1898(\rho_{R_{s0}R_{sh0}}) & 0.7657(\rho_{R_{s0}n_0}) & 0.7447(\rho_{R_{s0}I_{d0}}) & 0.4564(\rho_{R_{s0}I_{sh0}}) \\ -0.1896(\rho_{R_{sh0}R_{s0}}) & 1(\rho_{R_{sh0}R_{sh0}}) & -0.2119(\rho_{R_{sh0}n_0}) & -0.2048(\rho_{R_{sh0}I_{d0}}) & -0.1398(\rho_{R_{sh0}I_{sh0}}) \\ 0.7657(\rho_{n_0R_{s0}}) & -0.2119(\rho_{n_0R_{sh0}}) & 1(\rho_{n_0n_0}) & 0.9954(\rho_{n_0I_{d0}}) & 0.7090(\rho_{n_0I_{sh0}}) \\ 0.7447(\rho_{I_{d0}R_{s0}}) & -0.2048(\rho_{I_{d0}R_{sh0}}) & 0.9954(\rho_{I_{d0}n_0}) & 1(\rho_{I_{d0}I_{d0}}) & 0.7289(\rho_{I_{d0}I_{sh0}}) \\ 0.4564(\rho_{I_{sh0}R_{s0}}) & -0.1398(\rho_{I_{sh0}R_{sh0}}) & 0.7090(\rho_{I_{sh0}n_0}) & 0.7289(\rho_{I_{sh0}I_{d0}}) & 1(\rho_{I_{sh0}I_{sh0}}) \end{bmatrix} \tag{A9}$$

$$\begin{bmatrix} 1(\rho_{vv}) & -0.0103(\rho_{v\xi}) & -0.2163(\rho_{v\gamma}) \\ -0.0103(\rho_{\xi v}) & 1(\rho_{\xi\xi}) & 2.4735\times10^{-5}(\rho_{\xi\gamma}) \\ -0.2163(\rho_{\gamma v}) & 2.4735\times10^{-5}(\rho_{\gamma\xi}) & 1(\rho_{\gamma\gamma}) \end{bmatrix} \tag{A10}$$

Table 1 Electrical experimental test uncertainties

Equipment	Interval (resolution)	Interval	Range of reading	Uncertainty	Other
AutoLab	I:6×10^{-6} A	±3×10^{-6} A	±2 A	Accuracy:±0.2%	
	V:3×10^{-7} V	±1.5×10^{-7} V	±10 V		
Pyranometer(Kipp & Zohon CMP11)	A:12 μV/(Wm^{-2})	2.56 μV(Wm^{2})	285-2800 nm	Temperature change:<1%	Range: -40-80 °C
	B:8.89 μV(Wm^{-2})			Time change:<5s	4000 W/m^{2} max
	C:9.01 μV(Wm^{-2})				
Spectral Radiometer (Macam SR9910.V7)	1nm	0.5 m	24-800	±20°C Stability	-10-400 °C Operating range:
Silicon reference cell(Seaward Solar Survey 100)	1 W/m^{2}	0.5 W/m^{2}	100-1250 W/m^{2}		1±0.5°(res angles)
FLIRi7	0.1 °C	0.05 °C	-20-250 °C		9Hz, 75-13μm detection
IR Thermometer (Maplin TN439L0)	3 °C	1.5 °C	-25-265 °C	Area@Distance expansion	0.08m^{2}@0.6m
					0.13m^{2}@1m
Thermocouples (Type K, PTFE,1m,RS:363-0250)	3 °C	1.5 °C	-75-250 °C		
Thermocouple reader(Fluke 52 Series II)	0.1 °C	0.05°C	0-9999 °C		Resolution depends on thermocouple
Multimeter(Chauvin Arnoux CA5231)	V:0.01 mV	V:0.005 mV	0-1000 V		
	Ohms:0.1	0.05 Ohm	0-60 MOhm		

Table 2 Five parameters in electrical model and four constants in scaling law for bare monocrystalline PV cell 100516

Model	Parameter	Optimized value
Electric model	n_0	1.2626±0.0100
	$R_{s0}(\Omega)$	1.5273×10^{-2}±3.5401×10^{-3}
	$R_{sh0}(\Omega)$	4.9941×10^{3}±5.5244×10^{2}
	I_{sh0} (A)	3.6654×10^{-2}±6.23×10^{-5}
	I_{d0}(μA)	5.4370×10^{-4}±7.40×10^{-5}
	$\varepsilon_1(\%)$	0.6116±0.1211
Scaling law	ξ	1.1828±0.0047
	v	0.8041±0.0573
	γ	-11.8155±0.0748
	μ	2.5×10^{-5}
	$\varepsilon_2(\%)$	2.0520±0.1345

Table 3 Five parameters extracted for six monocrystalline PV modules under STC

PV module	n_0	R_{s0} (Ω)	R_{sh0} (Ω)	I_{sh0} (A)	I_{d0} (μA)	ε_1 (%)
BM60 265BB	90.6283 ±1.3360	0.2163 ±0.0032	1.299966×10^{5} $\pm3.0005\times10^{4}$	9.0717 ±0.0276	0.4079 ±0.0890	0.7069 ±0.2540
Hyundai S325TI	87.3248 ±0.0013	0.2206 ±0.0012	7.5612×10^{2} ±12.3022	8.5433 ±0.0025	1.5458×10^{-2} ±0.0009	0.8202 ±0.1054
Sanyo HIT215	123.8192 ±4.1438	0.4768 ±0.0181	1.5360×10^{4} ±4992.0169	5.5457 ±0.0481	0.6586 ±0.2882	2.2363 ±0.7608
Shell SM55	47.4443 ±1.4535	0.3021 ±0.0248	1.0998×10^{3} ±99.2738	3.4472 ±0.0201	9.0288×10^{-2} ±0.0096	1.9566 ±0.3743
SILVANTIS D330	99.7249 ±1.5862	0.2356 ±0.0043	2.7477×10^{3} ±249.3252	9.1624 ±0.0355	1.5862×10^{-1} ±0.0408	0.8616 ±0.3703
TSM270 DC05A	95.9918 ±2.2074	0.2210 ±0.0040	2.4959×10^{4} $\pm5.0048\times10^{3}$	9.3446 ±0.0430	1.4484 ±0.6560	1.0276 ±0.3878

Table 4 Four parameters in scaling law for six monocrystalline PV modules

PV module	ξ	v	γ	μ	ε_2 (%)
BM60 265BB	0.8367 ±0.0121	0.8963 ±0.0396	-11.5675 ±0.0647	4.75×10^{-3}	4.0355 ±0.3373
Hyundai S325TI	0.9148 ±0.0161	0.4737 ±0.1299	-8.8661 ±0.0639	4.75×10^{-3}	4.3890 ±0.3742
Sanyo HIT215	1.0652 ±0.0093	1.0298 ±0.01523	-18.7262 ±0.1035	1.68×10^{-3}	6.8303 ±0.5706
Shell SM55	0.92573 ±0.0073	0.5231 ±0.0413	-12.4158 ±0.2203	1.75×10^{-3}	17.9170 ±3.0611
SILVANTIS D330	0.9023 ±0.0015	0.5018 ±0.0126	-11.2650 ±0.1827	4.75×10^{-3}	7.6404 ±1.1420
TSM270 DC05A	0.80761 ±0.0096	0.5713 ±0.0938	-17.1618 ±0.0615	4.75×10^{-3}	5.0755 ±0.2419
Average	0.9087	0.6583	-13.3337	3.74×10^{-3}	7.6480

Table 5 Parameters in scaling law for PV cell 100516 with and without CCPC

Case	Parameters	*CR*		Effect of CCPC (%)	Mean effect of CCPC (%)	Approximate correction (%)
		1	3.6			
Case 1	ξ	1.1826 ±0.0045	1.2441 ±0.0031	5.20	3.64	5
	v	0.8041 ±0.0597	0.9009 ±0.0576	12.04	12.33	15
	γ	-11.8155 ±0.0681	-7.7028 ±0.0340	-34.81	-21.92	-20
	μ	2.5×10^{-5}	2.5×10^{-5}	0	0	0
Case 2	ξ	1.2255 ±0.0068	1.2509 ±0.0042	2.08	Mean effect of CCPC on a parameter is the arithmetic mean of the effects in Case 1 & 2 for that parameter.	
	v	0.8021 ±0.0861	0.9034 ±0.0547	12.63		
	γ	-8.5975 ±0.0652	-7.8203 ±0.1027	-9.04		
	μ	2.5×10^{-5}	2.5×10^{-5}	0		

1) In Case 1, the I-V experimental data of bare PV cell or PV cell with CCPC are used separately for determining five parameters in electric model; in Case 2, the I-V experimental data of both bare cell and cell with CCPC are used simultaneously.

2) The effect of CCPC on three constants is defined as the percentage of the difference in a parameter

Table 6 Five parameters in electric model and four constants in scaling law for bare PV cell IQE PCB 2 without CCPC

Model	Parameter	Value optimized
Electric model	n_0	5.1745±0.0834
	$R_{s0}(\Omega)$	$2.1408\times10^{-3}\pm5.4993\times10^{-4}$
	$R_{sh0}(\Omega)$	$7.9889\times10^{4}\pm5.3355\times10^{3}$
	I_{sh0} (A)	$4.0775\times10^{-3}\pm9.7730\times10^{-5}$
	I_{d0} (μA)	$2.8836\times10^{-4}\pm6.4214\times10^{-5}$
	$\varepsilon_1(\%)$	2.9847±0.5587
Scaling law	ξ	1.1111±0.0012
	v	0.6544±0.1904
	γ	-5.0016±0.0435
	μ	3×10^{-6}
	ε_2 (%)	1.8795±0.0591

Table 7 Four parameters in scaling law for PV cell IQE2PCB1504 with and without CCPC

Case	Parameter	*CR*		Effect of CCPC (%)	Mean effect of CCPC (%)
		1	4		
Case 1	ξ	1.1111	1.1412	2.71	1.44
	v	0.6544	0.6560	0.24	1.13
	γ	-5.0016	-6.2778	25.52	8.98
	μ	3×10^{-6}	3×10^{-6}	0	0
Case 2	ξ	1.1341	1.1360	0.17	
	v	0.6430	0.6559	2.01	
	γ	-4.5391	-4.1958	-7.56	
	μ	3×10-6	3×10^{-6}	0	

Notation is the same as that of Table 5, but E_0 =0.663eV for Ge is in the models.

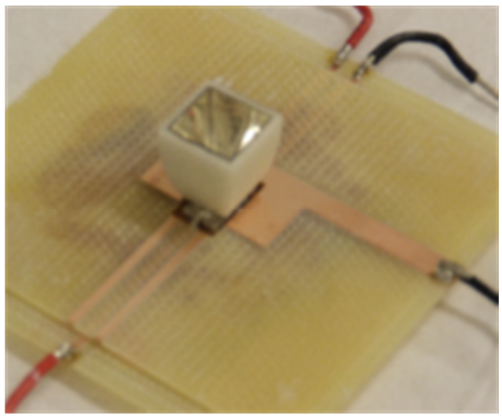

Fig. 1 Picture of integrated monocrystalline CPV-TE device with CCPC optics

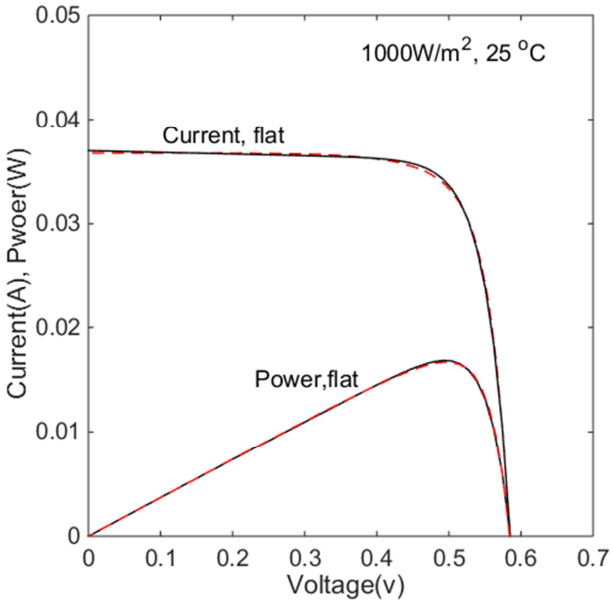

Fig. 2 Comparison of the I-V and power-V curves between the prediction (solid line) and the measurement (dashed line) at STC (1000 W/m^2, 25 °C) for a bare flat PV cell 100516

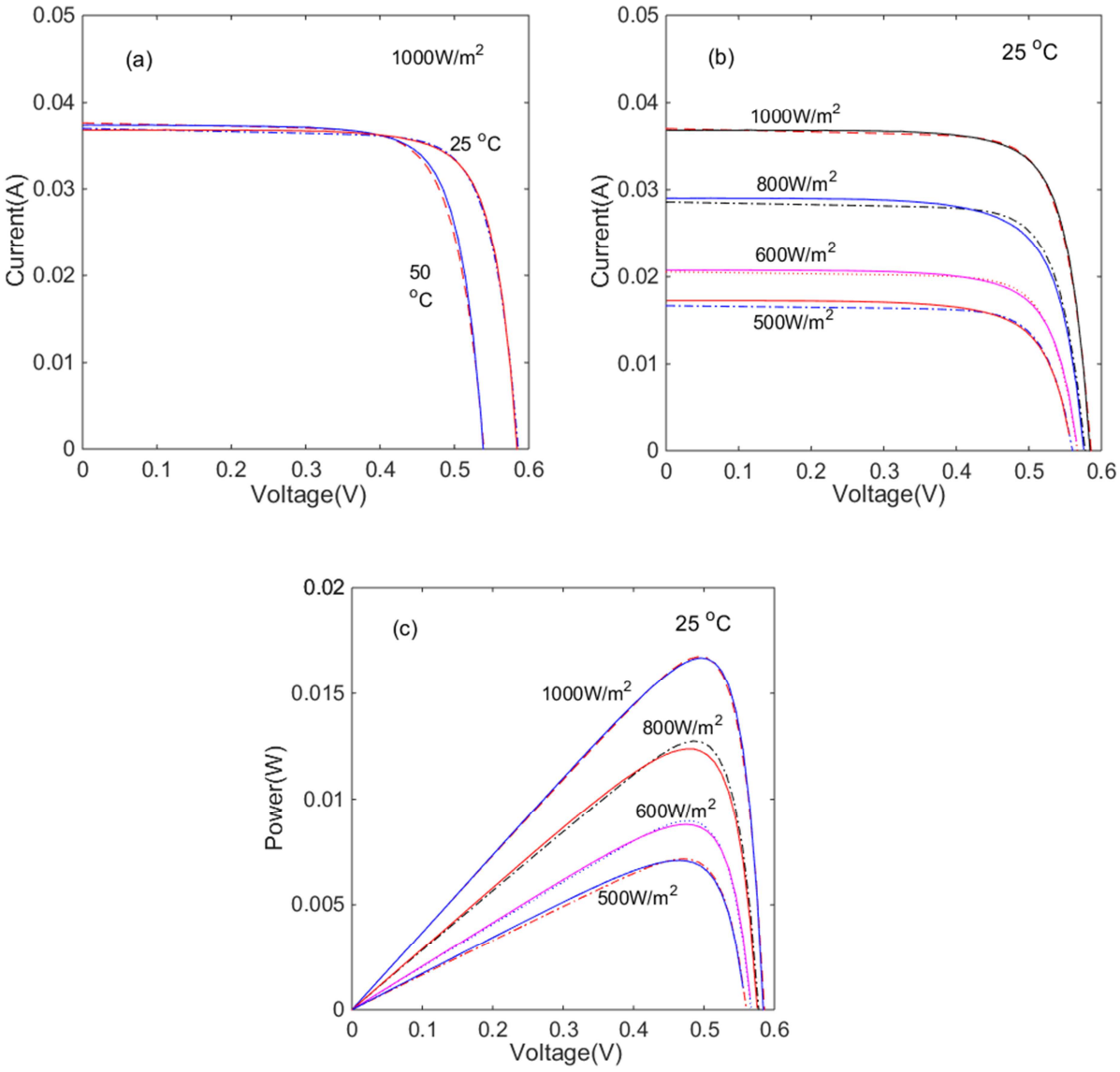

Fig. 3 Comparison of the I-V and P-V curves between the prediction (solid line) and the measurement (dashed line) at 1000 W/m^2 and variable cell temperature (a), 25 ^{o}C and variable irradiance (b) and (c)

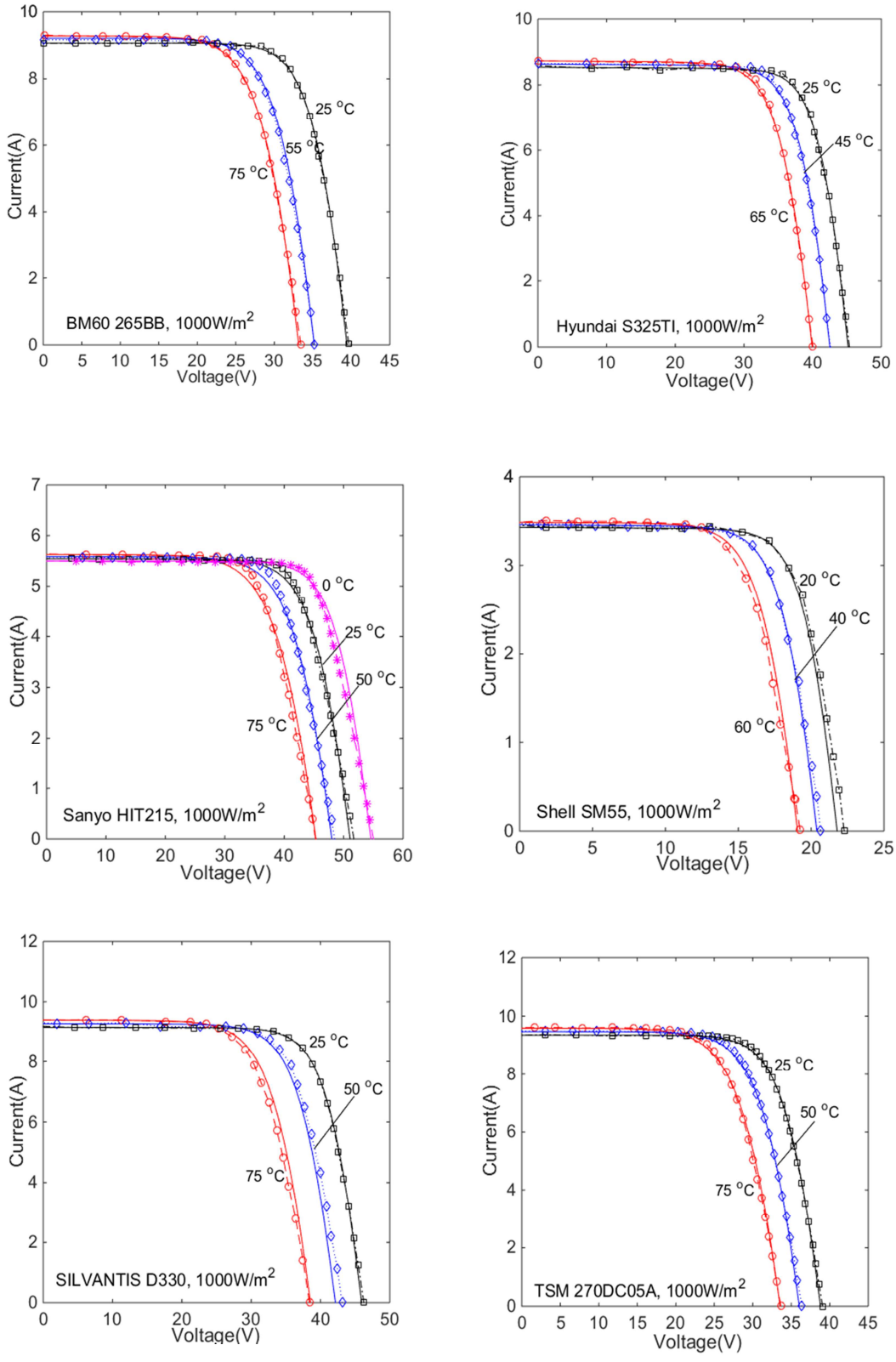

Fig. 4 Comparison of the I-V curves predicted (solid line) by the scaling laws produced and those from literature (dashed line and symbol) at various cell temperatures and 1000 W/m^2 irradiance for six PV modules

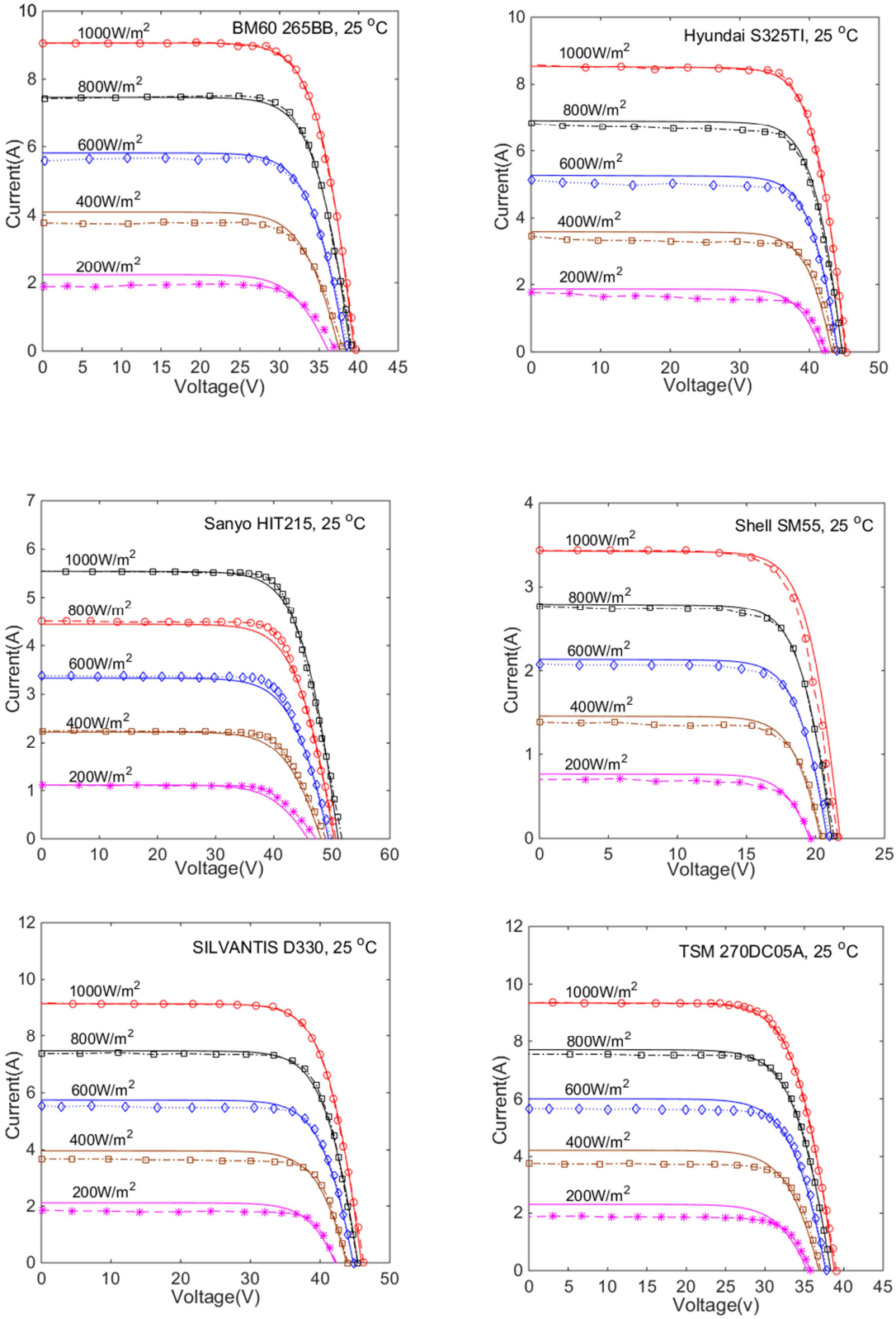

Fig. 5 Comparison of the predicted I-V curves (solid line) by the scaling law produced and those from literature (dashed line and symbol) at various irradiances and constant cell temperature 25°C for six PV modules

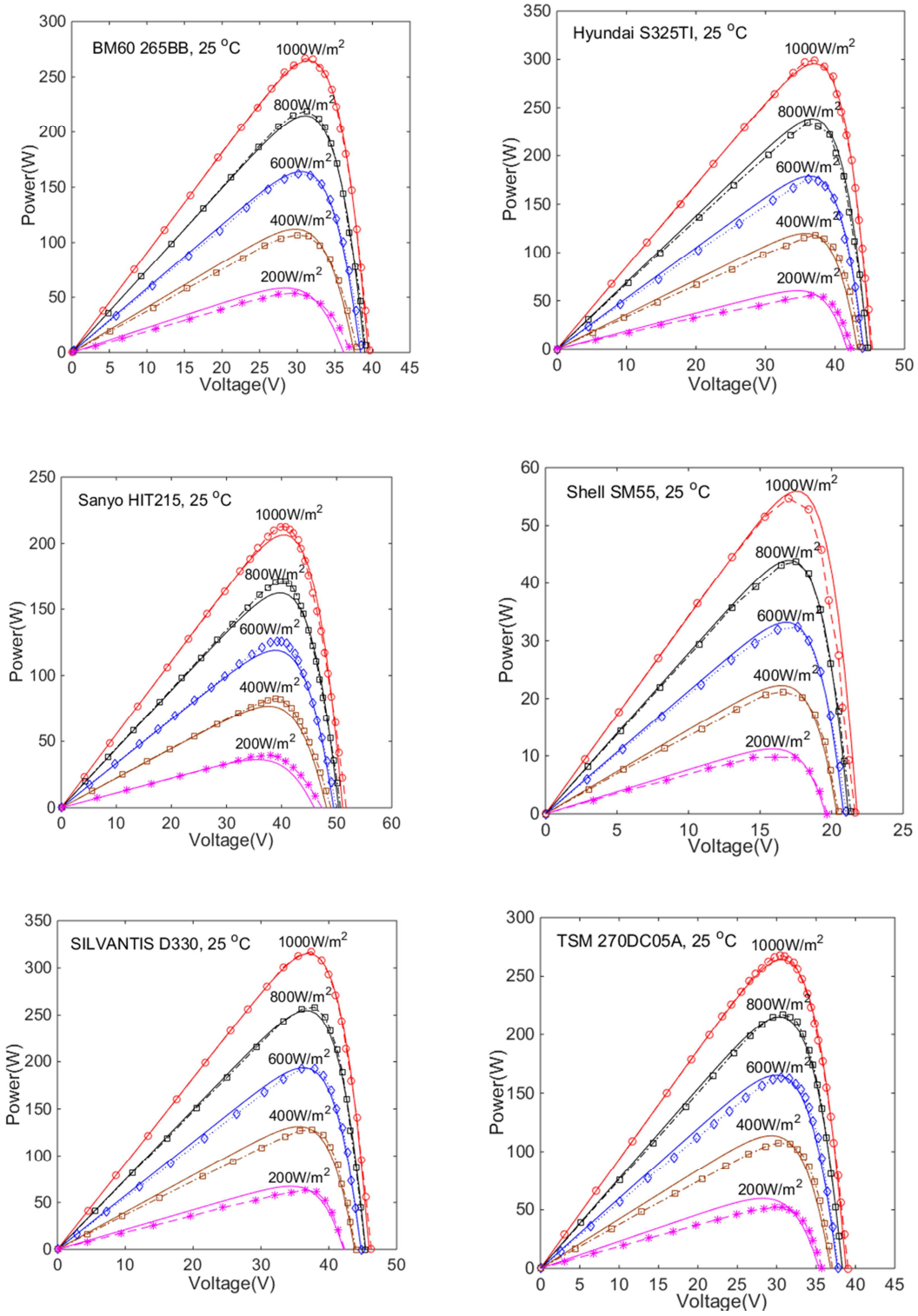

Fig. 6 Comparison of the predicted power curves (solid line) by the scaling law produced and the measurements from literature (dashed line and symbol) various irradiances and constant cell temperature 25 °C for six PV modules

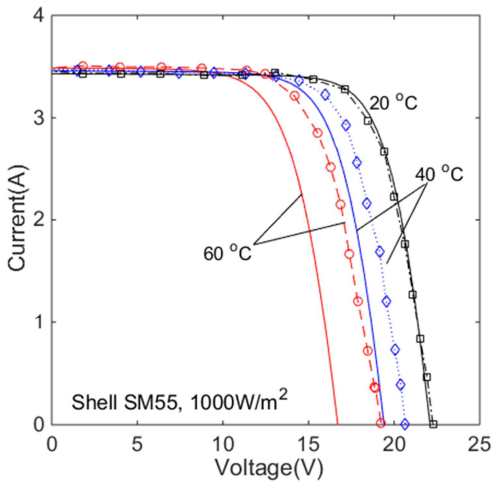

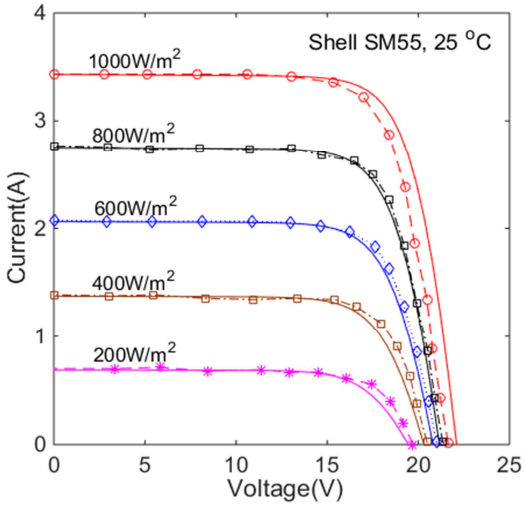

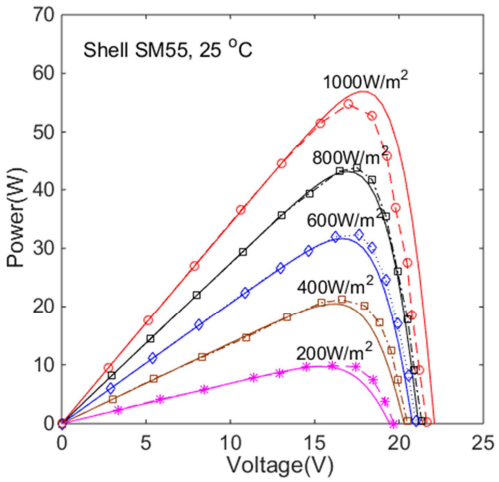

Fig. 7 Comparison of the I-V and power-V curves of PV module Shell SM55 between the prediction (solid line) and the measurements (dashed line and symbol) at STC and off-STC, the predictions are made by using the existing scaling laws expressed with Eq. (15)

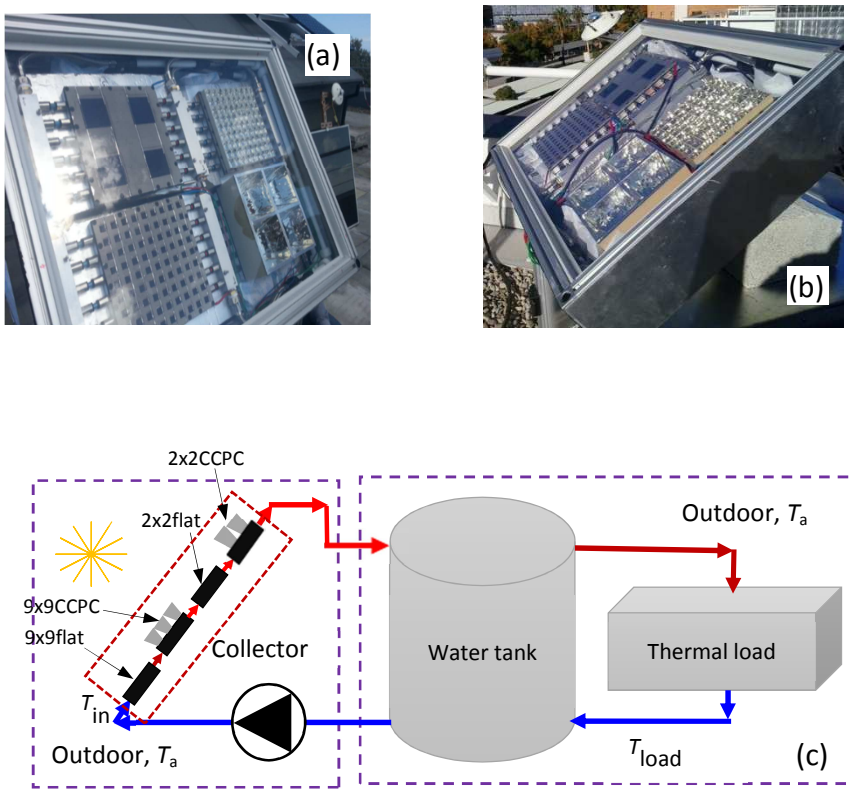

Fig. 8 PV/T roof-top system picture (a) and in Jaen (b) as well as the system block diagram (c)

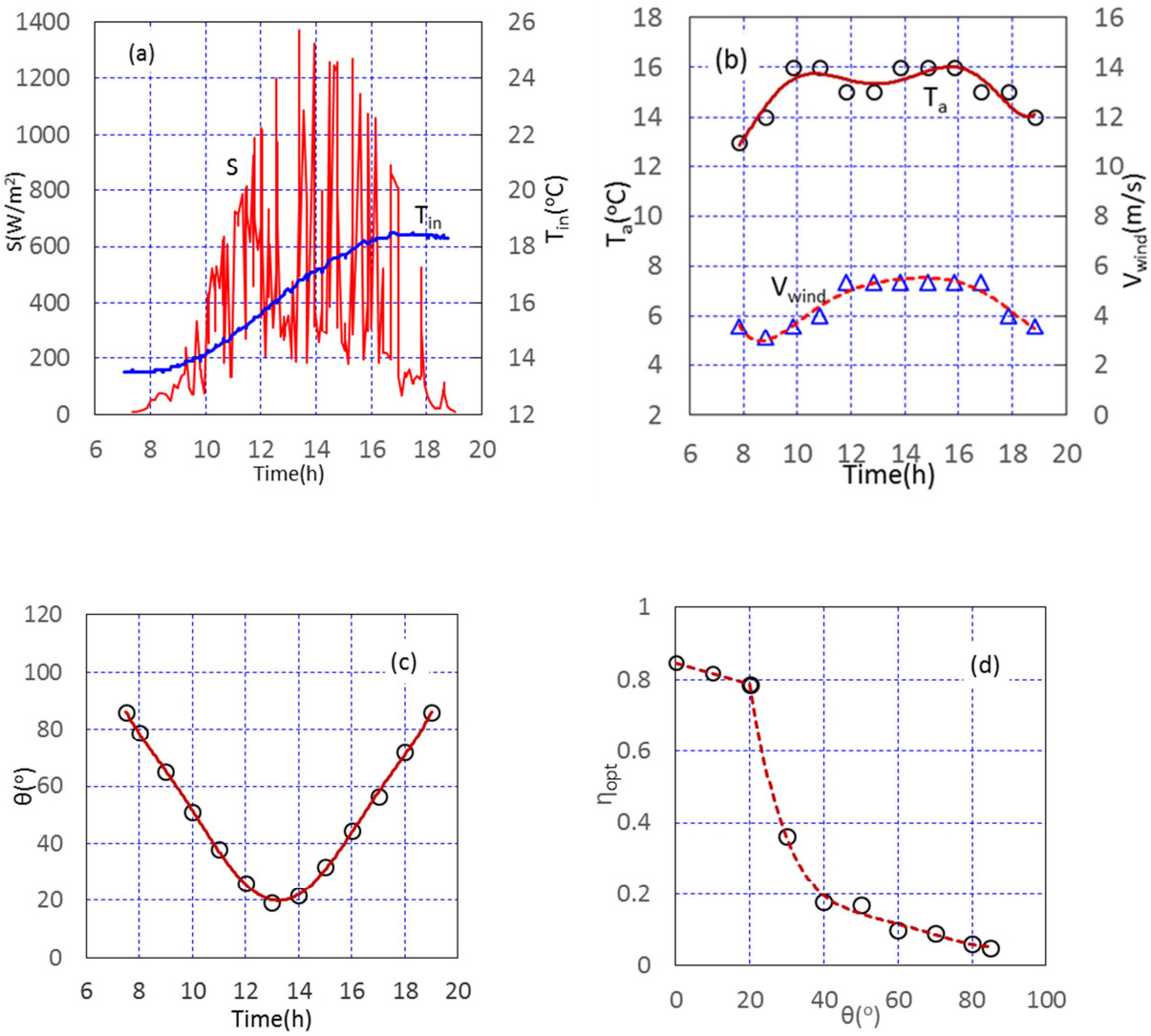

Fig. 9 Outdoor measured solar irradiance, S, water temperature at the inlet of heat exchanger in 9x9flat module, T_{in}, ambient temperature, T_a, wind speed and incidence, V_{wind}, in the day of 17 September 2015 in Penryn, England, as well as CCPC optical efficiency in terms of incidence, η_{opt}, predicted by ANSYS CFX, (a) irradiance and water temperature, (b) ambient temperature and wind speed, (c) incidence in terms of time, (d) optical efficiency as a function of incidence

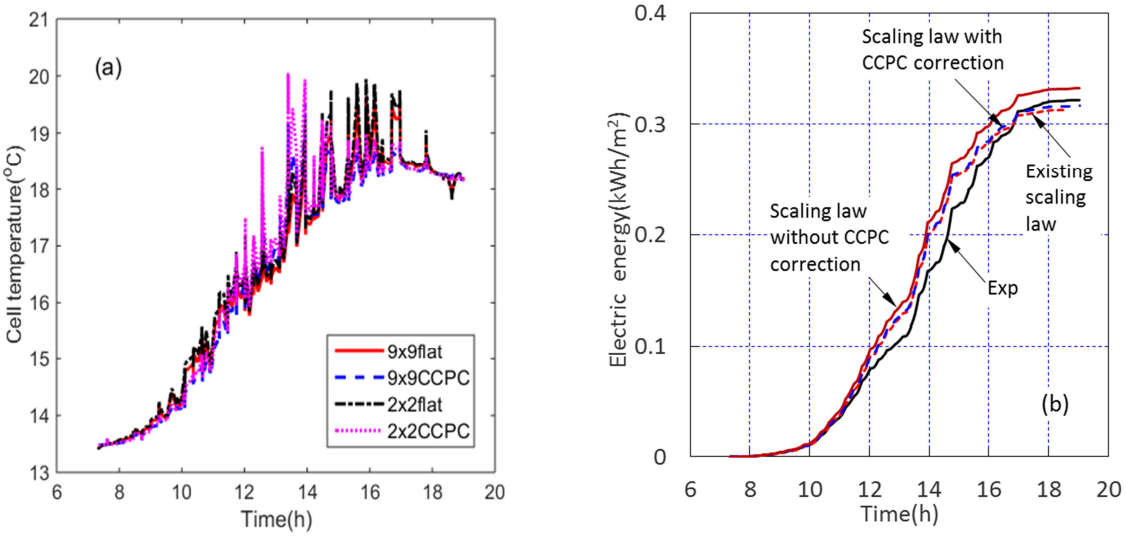

Fig. 10 Predicted cell temperature in 9×9flat, 9×9 CCPC, 2×2flat and 2×2 CCPC modules (a) and electric energy obtained by the four modules (b) at a flow rate of 4.3 L/min

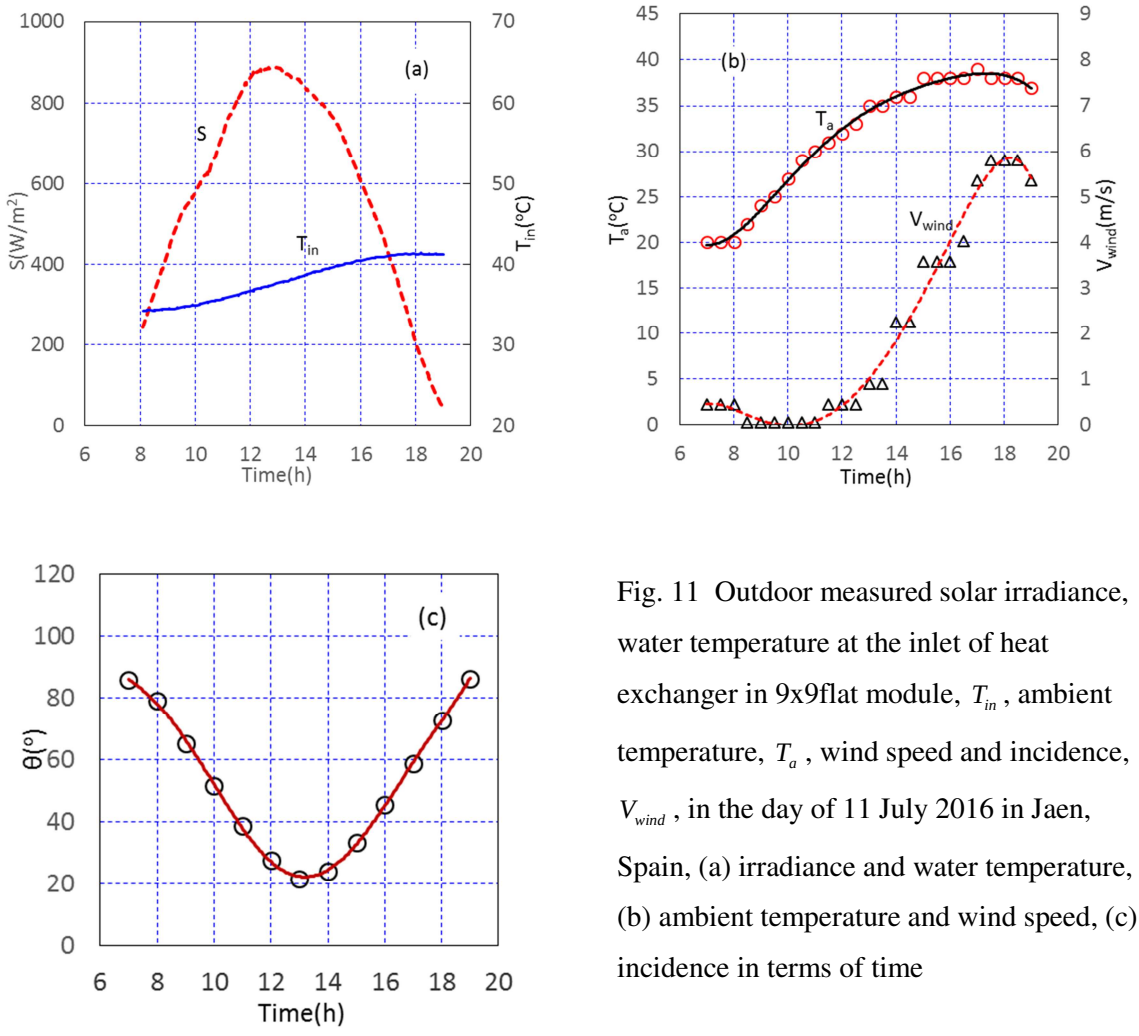

Fig. 11 Outdoor measured solar irradiance, S, water temperature at the inlet of heat exchanger in 9x9flat module, T_{in}, ambient temperature, T_a, wind speed and incidence, V_{wind}, in the day of 11 July 2016 in Jaen, Spain, (a) irradiance and water temperature, (b) ambient temperature and wind speed, (c) incidence in terms of time

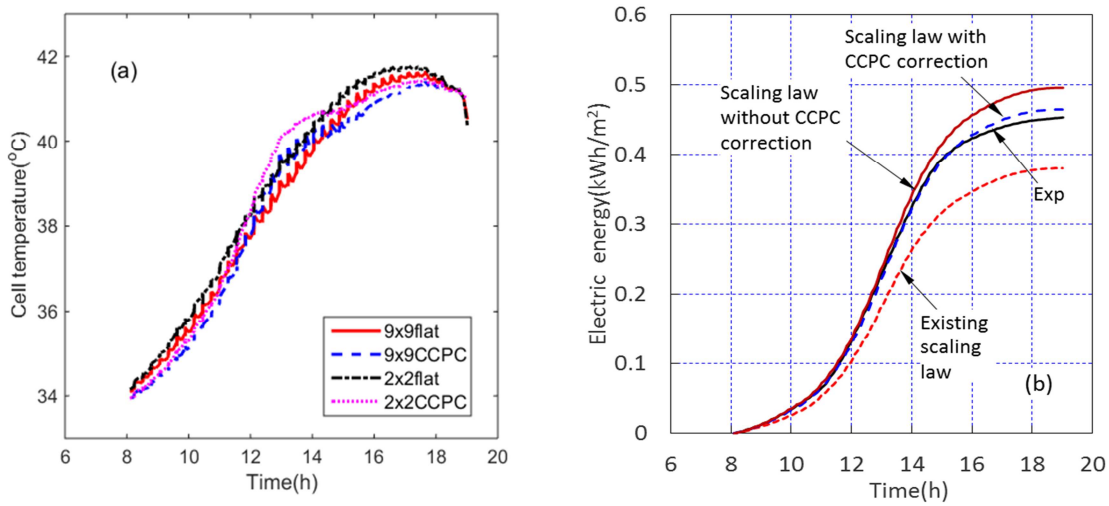

Fig. 12 Predicted cell temperature in 9×9flat, 9×9CCPC, 2×2flat and 2×2 CCPC modules (a) and electric energy obtained by the four modules (b) at a flow rate of 1.24 L/min